RESONANCE SCATTERING PHASE SHIFTS ON A NON–REST FRAME LATTICE

K. Rummukainen and Steven Gottlieb

Department of Physics, Indiana University,
Bloomington, IN 47405, USA

Abstract

Many low energy hadrons, such as the rho, can observed as resonances in scattering experiments. A proposal by Lüscher enables one to determine infinite volume elastic scattering phases from the two-particle energy spectrum measured from finite periodic lattices. In this work, we generalize the formalism to the case where the total momentum of the particles is non-zero; i.e.,the lattice frame is not the center-of-mass frame of the scattering particles. There are several advantages to this procedure including making a wider variety of center of mass energies accessible with a fixed lattice volume, and making the avoided level crossing in a P-wave decay occur with a smaller volume.

The formalism is tested with a simple lattice model of two fields with different masses and a 3-point coupling in $3 + 1$ dimensions. We find remarkable agreement between the rest-frame and non-rest-frame scattering.

1 Introduction

Numerical lattice simulations have been fairly successful in calculating many low energy properties of QCD, the most fundamental being the mass spectrum of the lightest hadrons [1]. However, most hadronic states are resonances that cannot be fully described without scattering with stable asymptotic states. A well-known example of this is the ρ-meson, which appears as a resonance in the elastic $\pi\pi \to \pi\pi$ scattering in the angular momentum $l = 1$ and isospin $I = 1$ channel. In fact, the calculation of the mass ratio of the nucleon and ρ has been a persistent problem for lattice calculations and only recently has there been evidence that the correct ratio emerges in the continuum limit [2, 3]. This has been demonstrated in the valence or quenched approximation where the ρ cannot decay. Most current dynamical quark calculations are done in a regime where the pions are so heavy that the rho cannot decay, so it is not that likely that this effect has played in an important role in the dynamical quark calculations [4]; however, as the chiral limit is approached this may become an important practical matter.

Although hadronic coupling constants, which require calculation of 3-point functions, have been studied on the lattice quite some time ago [5], only recently have there been attempts to resolve hadronic scattering phases, which require 4-point functions. Most of the results are for meson–meson and meson–nucleon scattering lengths at zero relative momentum [6–10]. In the resonance channel $\pi\pi$–ρ the two pions are in the $l = 1$ state and have non-vanishing relative momentum. The resonance has not yet been observed on the lattice, despite an attempt by the MILC collaboration [11].

Elastic scattering involves at least four asymptotic states, which, in the case of QCD, are themselves bound states of fundamental quark and gluon fields. Because the lattice simulations are by necessity restricted to quite small and usually periodic physical volumes, the direct observation of freely propagating asymptotic states is not possible. At best, the linear dimensions of the lattices are only a few times the interaction length.

In a series of papers Lüscher [12, 13, 14] developed a method that enables one to measure the scattering phase shifts from standard lattice Monte Carlo simulations. The method relates the two-particle energy eigenstates on a finite periodic box to the infinite-volume asymptotic scattering states. The lattice measurement requires the determination of the two-particle energy spectrum, a task readily performed with lattice Monte Carlo methods. The finite volume of the lattice is not a disadvantage in this method, on the contrary, it is used to probe the system, and simulations with several different volumes are combined in order to obtain maximal knowledge about the phase shift.[1] In two dimensions, the method has been applied to O(3) nonlinear σ-model [18] and to a model consisting of two coupled Ising spins [19]; it has also been applied to 3-dimensional QED [20, 21] and to 4-dimensional O(4) ϕ^4 theory [22]. First attempts to apply the method to fermion-fermion

---

[1]Related proposals for measuring the resonance parameters on a finite lattice have been brought forward by Michael [15], Wiese [16] and DeGrand [17].

scattering in the Gross-Neveu model have been made [23].

In Lüscher's formalism the center of mass of the scattering particles is stationary with respect to the lattice, i.e.,the two particles have opposite lattice frame momenta. In this paper we generalize the formalism to encompass elastic scattering with *non-zero total momentum*. This has several advantages: first, since both the zero-momentum and non-zero momentum sectors can be measured simultaneously, one lattice run may yield two separate data points with a small cost in computer time. (How small or large that cost may be is model dependent and depends the ratio of update time to measurement time.) Second, the zero-momentum and non-zero momentum data tend to complement each other: a much smaller volume range is needed in order to obtain a good description of the phase shift as a function of the center of mass momentum. Third, as can be seen in figure 1, for a decay where the outgoing particles must have relative angular momentum as in $\rho \to \pi\pi$, the avoided level crossing in the non-zero momentum sector occurs for a smaller lattice size ($L/a \approx 15$ as opposed to $L/a \approx 35$, for the parameters chosen in the figure). Fourth, for channels that require a vacuum subtraction in the zero momentum sector, the non-zero momentum sector tends to have smaller statistical errors, since no subtraction is required.

We apply the method to a simple 4-dimensional test model. The model contains two scalar fields: a light mass field ϕ and a heavier field ρ. Our goal is to investigate the scattering amplitude of the infinite volume elastic $\phi\phi \to \phi\phi$ scattering process. The mass of the ϕ field cannot be too small: in order to reduce the finite volume polarization effects (self-interactions of the particles "around the world") the linear dimension L of the lattice should be at least a few times the correlation length $\xi = 1/m_\phi$. The field ρ has a mass $m_\rho \leq 2m_\phi$; with the introduction of the 3-point $\rho\phi^2$ coupling the ρ particle is rendered unstable and it appears as a resonance in the $l = 0$ scattering channel. Our model is simpler than nature where a charged pion field has a derivative coupling to the spin-1 rho, $\pi^2 \partial_\mu \pi \rho^\mu$, resulting in a resonance in the $l = 1$ channel.

In the center of mass system, the scattering amplitude T of the elastic scattering of two identical spin-0 bosons is a function of the absolute value of the momenta of the incoming particles p and the scattering angle θ. The standard form of the partial wave decomposition of the scattering amplitude is

$$T(p, \theta) = \frac{16\pi W}{p} \sum_{l=0}^{\infty} (2l + 1) P_l(\cos\theta) t_l(p) \,, \tag{1}$$

where $W = 2\sqrt{p^2 + m_\phi^2}$ is the total energy of the scattering particles. Assuming a unitary S-matrix the partial amplitudes $t_l(p)$ are expressed with the phase shift $\delta_l(p) \in \mathbf{R}$ as

$$t_l(p) = \frac{1}{2i}(e^{i2\delta_l} - 1). \tag{2}$$

Due to the Bose symmetry t_l vanish for odd l.

2

In this work we are primarily interested only in the $l = 0$ channel, where the resonance appears. We measure the scattering phase shift both in the zero and non-zero total momentum sectors and find an excellent agreement between the momentum sectors and with the perturbative ansatz.

The rest of this paper is organized as follows: in sec. 2 we discuss the general properties of two-particle states on a torus for free and then interacting particles. In sec. 3, we give the details of the Monte Carlo simulations of our model, including the algorithms and parameters used, the correlators calculated on the configurations, the energy spectrum of various one- and two-particle levels, and the extraction of the phase shift and resonance parameters. In sections 4 and 5 we discuss the theoretical aspects of the method: section 4 extends Lüscher's formalism to the non-rest frame case and derives the relationship for the phase shift, eq. (17), and sec. 5 details the symmetry considerations that may be used to simplify the wave functions for the energy eigenstates. Brief conclusions are presented in sec. 6.

2　Two-particle states on a torus

In this section we introduce the formalism necessary for calculating the scattering phase shifts in a periodic 3-dimensional box. Although at the end the results will be applied to discrete periodic lattices, at this stage we assume continuous space-time; and correct for discreteness of the lattice structure later. The formulae given here are sufficient for analyzing the lattice data. The derivation of the basic equation (18) is done in section 4; the reading of this section is not necessary for the analysis of the lattice data. We follow the basic formalism and notation introduced by M. Lüscher [12, 13], generalizing it to encompass the non-zero total momentum sector.

2.1　Non-interacting particles

Let us first consider a system of two *non-interacting* identical bosons (ϕ) of mass $m_\phi > 0$ in a cubic box of volume L^3 with periodic boundary conditions. The total energy of the system in the rest frame of the box, which we shall call the laboratory frame or the lattice frame (L) is

$$W_{\mathrm{L}} = \sqrt{\mathbf{p}_1^2 + m_\phi^2} + \sqrt{\mathbf{p}_2^2 + m_\phi^2}, \tag{3}$$

where $\mathbf{p}_i$ are the 3-momenta of the particles. In the center of mass frame (CM) the energy is

$$W_{\mathrm{CM}} = 2\sqrt{p^{*2} + m_\phi^2}, \tag{4}$$

with $\mathbf{p}^* = \mathbf{p}_1^* = -\mathbf{p}_2^*$, $p^* = |\mathbf{p}^*|$. We denote here the center of mass momenta with an asterisk (*). In the laboratory frame, the center of mass is moving with velocity $\mathbf{v}$, and

the momenta $\mathbf{p}_i$ and $\mathbf{p}^*$ are related by the standard Lorentz transformation

$$\mathbf{p}^* = \vec{\gamma}\,(\mathbf{p}_1 - \mathbf{v}\sqrt{\mathbf{p}_1^2 + m_\phi^2}) = -\vec{\gamma}\,(\mathbf{p}_2 - \mathbf{v}\sqrt{\mathbf{p}_2^2 + m_\phi^2})\,, \tag{5}$$

where we have defined

$$\gamma = \frac{1}{\sqrt{1 - \mathbf{v}^2}} \tag{6}$$

and we have used the shorthand notation

$$\vec{\gamma}\,\mathbf{p} = \gamma \mathbf{p}_\| + \mathbf{p}_\perp, \quad \vec{\gamma}^{\,-1}\mathbf{p} = \gamma^{-1}\mathbf{p}_\| + \mathbf{p}_\perp, \tag{7}$$

where $\mathbf{p}_\|$ and $\mathbf{p}_\perp$ are components of $\mathbf{p}$ parallel and perpendicular to the center of mass velocity: $\mathbf{p}_\| = (\mathbf{p} \cdot \mathbf{v})\mathbf{v}/v^2$ and $\mathbf{p}_\perp = \mathbf{p} - \mathbf{p}_\|$. Let the laboratory frame total momentum $\mathbf{P} = \mathbf{p}_1 + \mathbf{p}_2$; then, using eq. (5), the velocity of the center of mass can be written as

$$\mathbf{v} = \mathbf{P}/W_\mathrm{L} \tag{8}$$

and the center of mass and laboratory frame energies are related by

$$W_\mathrm{L} = \sqrt{\mathbf{P}^2 + W_\mathrm{CM}^2} = \sqrt{\mathbf{P}^2 + 4(p^{*2} + m_\phi^2)}\,. \tag{9}$$

Using eq. (9) we can obtain the center of mass momentum p^{*2} in terms of the laboratory frame momenta $\mathbf{p}_i$:

$$p^{*2} = \frac{1}{4}(W_\mathrm{L}^2 - \mathbf{P}^2) - m_\phi^2. \tag{10}$$

It is illustrative to consider the energy levels of the system consisting of two non-interacting particles. In this case, the torus quantizes the laboratory frame momenta $\mathbf{p}_i$ to values

$$\mathbf{p}_i = \frac{2\pi}{L}\mathbf{n}, \quad \mathbf{n} \in \mathbf{Z}^3. \tag{11}$$

The total momentum is similarly quantized. Note that the lowest values of $\mathbf{p}_i^2$ are evenly spaced: $p_i^2/(2\pi/L)^2 = 0, 1, 2, \ldots$; the first skipped value is 7. When the laboratory frame total momentum $P = |\mathbf{P}| = 0$, the momenta of the two particles are opposite $\mathbf{p}_2 = -\mathbf{p}_1$ and the levels are given by eqs. (3) and (11):

$$W_\mathrm{L} = W_\mathrm{CM} = 2\sqrt{m_\phi^2 + (\mathbf{n}2\pi/L)^2}, \qquad \mathbf{n} \in \mathbf{Z}^3\,. \tag{12}$$

In figure 1 we show the seven lowest $P = 0$ levels with solid lines as functions of L, where L is given in units of an arbitrary length scale a. The mass of the particles is fixed to $m_\phi = 0.3/a$. The lowest level, corresponding to two particles at rest, is the horizontal line at $W = 0.6/a$.
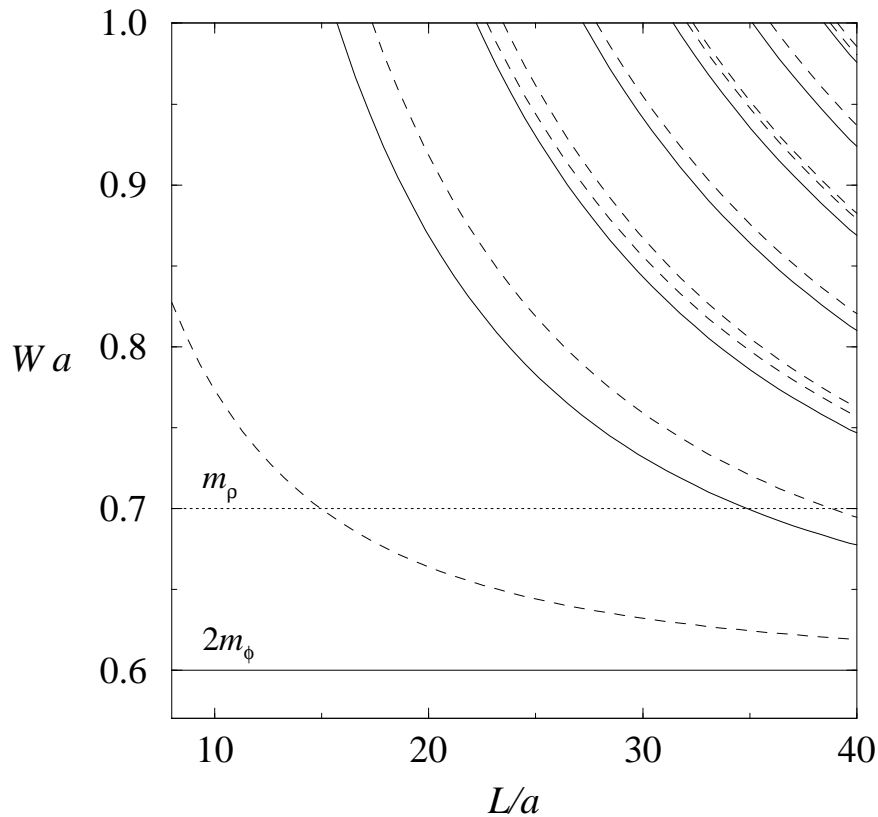
4

Figure 1: Center of mass energy levels of a system of two non-interacting particles of mass $0.3/a$ as functions of the system size L. Solid lines correspond to the zero total momentum sector $P = 0$, and dashed lines to sector $P = 2\pi/L$.

The lowest non-zero value for P is $(2\pi/L)$ along some coordinate axis. For concreteness, let us choose $\mathbf{P} = \mathbf{e}_3 2\pi/L$; now the center of mass energy can be solved from eq. (9):

$$W_{\text{CM}}^2 = W_{\text{L}}^2 - \mathbf{P}^2 = \left[\sqrt{\mathbf{p}_1^2 + m_\phi^2} + \sqrt{\mathbf{p}_2^2 + m_\phi^2} \right]^2 - (2\pi/L)^2 \qquad (13)$$

where $\mathbf{p}_1 = (\mathbf{n} + \mathbf{e}_3)\, 2\pi/L$ and $\mathbf{p}_2 = -\mathbf{n}2\pi/L$ for some $\mathbf{n} \in \mathbf{Z}^3$. In figure 1 we show the lowest center of mass energy levels with dashed lines; they correspond, from the lowest upwards, to vectors

$$\mathbf{n} = (0,0,0),(0,1,0),(0,0,1),(1,1,0),(0,1,1),(0,2,0),(1,1,1),(1,2,0),\ldots \qquad (14)$$

where we have chosen $n_2 \geq n_1 \geq 0$; momentum states with $(n_1, n_2) \to (\pm n_1, \pm n_2)$ or $(\pm n_2, \pm n_1)$ have degenerate energy levels.

It should be noted that the center of mass frame is not unique, because the velocity of the center of mass for each two-particle state depends on the energy W_{L} according to

eq. (8). Thus, even for fixed L, we cannot make a boost to *the* center of mass frame and measure the energy levels there. The most convenient choice is to perform all the measurements in the laboratory frame, where all the levels have the same total momentum. From eqs. (8) and (13) we note that the velocity of the center of mass frame with respect to the laboratory frame is given by $v = [1 + (W_{CM}L/2\pi)^2]^{-1/2}$.

When comparing the sectors $P = 0$ and $P = (2\pi/L)$ we note that for each $P = 0$ level there is a $P \neq 0$ level with a slightly higher energy. The largest difference is between the lowest levels, where the $\mathbf{p}_1 = \mathbf{p}_2 = 0$ level does not have any volume dependence. Occasionally there appear two closely spaced levels in the $P = (2\pi/L)$ sector. This is a relativistic effect, that lifts the degeneracy of some of the momentum states. As an example, let us consider two-particle states with momenta $(p_1 = 4\pi/L, p_2 = 2\pi/L)$ and $(p_1 = 2\sqrt{2}\,\pi/L,\ p_2 = 2\sqrt{3}\,\pi/L)$. These states correspond to vectors $\mathbf{n} = (0,0,1)$ and (1,1,0) in eq. (13), which gives them non-degenerate laboratory frame energies, but both have non-relativistic kinetic energy

$$W_{\text{L,nonrel}} = \frac{p_1^2 + p_2^2}{2m_\phi} = 5\frac{(2\pi/L)^2}{2m_\phi}\,. \tag{15}$$

The next non-zero total momentum sector is $P = \sqrt{2}\,2\pi/L$, corresponding, for example, to $\mathbf{P} = (\mathbf{e}_1 + \mathbf{e}_2)2\pi/L$. In this case already the lowest two 2-particle energy levels are nearly degenerate.

2.2   Interacting particles

The utility of the $P \neq 0$ momentum sectors on a lattice becomes evident when we consider resonance scattering. To illustrate this let us introduce a new particle (ρ) with mass m_ρ, $2m_\phi < m_\rho < 4m_\phi$, and with the same laboratory frame momentum as the two ϕ particles. In figure 1 the ρ particle energy level is shown with a horizontal dotted line $W = m_\rho$; we have arbitrarily chosen $m_\rho = 0.7/a$. The ρ energy level is intersected by 2ϕ energy levels at various system sizes L. If we now introduce a small 3-point $\phi\phi - \rho$ interaction, ρ becomes unstable. Due to the interaction the energy eigenstates are a mixture of ρ and 2ϕ states. This is evident as *avoided level crossings* in the energy levels; in figure 1 the interaction is absent, but the avoided crossings would take place near the intersections of the ρ and 2ϕ levels. For the $P = 0$ sector the first crossing occurs at $L = 35\,a$, whereas for the $P = 2\pi/L$ sector the first crossing is already at $L = 15\,a$. In numerical lattice simulations this difference means that the avoided level crossing can be observed on lattices with more than 10 times smaller spatial volume.

In our calculations the ϕ^4 interaction in action (21) is strong enough so that the two-particle energy levels are not close to the free particle levels even far away from the level crossings. When the interaction is turned on the momenta $\mathbf{p}_i$ of the individual particles are not good quantum numbers and the quantization condition (11) is not valid any

more. On the other hand, since the interaction depends only on the relative position of the particles, the total momentum is conserved and is still quantized by eq. (11). For compactness, we shall label the different **P**-sectors with a vector $\mathbf{d} \in \mathbf{Z}^3$, defined through

$$\mathbf{P} = \mathbf{d}\frac{2\pi}{L}. \tag{16}$$

Assuming that the interaction is localized to a region smaller than L, the main result of section 4 is that the energy spectrum is still given by the formulae (3), (4) and (9) but instead of the the momentum quantization condition eq. (11) we have a relation involving the scattering phase shifts δ_l, where l labels the angular momentum of the scattering channel. Assuming that the phase shifts δ_l with $l = 2, 4, 6,\ldots$ are negligible in the energy range of interest, the phase shift δ_0 is related to the momentum p^* by

$$\delta_0(p^*) = -\phi^{\mathbf{d}}(q) \bmod \pi, \quad q = \frac{p^*L}{2\pi} \tag{17}$$

where $\phi^{\mathbf{d}}$ is a continuous function defined by the equation

$$\tan(-\phi^{\mathbf{d}}(q)) = \frac{\gamma q \pi^{3/2}}{Z_{00}^{\mathbf{d}}(1; q^2)} \qquad \phi^{\mathbf{d}}(0) = 0. \tag{18}$$

Function $Z_{00}^{\mathbf{d}}$ is generalized zeta function, and is formally given by

$$Z_{00}^{\mathbf{d}}(s; q^2) = \frac{1}{\sqrt{4\pi}} \sum_{\mathbf{r} \in P_{\mathbf{d}}} (\mathbf{r}^2 - q^2)^{-s}, \tag{19}$$

where the set $P_{\mathbf{d}}$ is

$$P_{\mathbf{d}} = \{\mathbf{r} \in \mathbf{R}^3 | \mathbf{r} = \vec{\gamma}^{-1}(\mathbf{n} + \mathbf{d}/2), \ \mathbf{n} \in \mathbf{Z}^3\}. \tag{20}$$

The expansion (19) is convergent when $\mathrm{Re}\, s > 3/2$, but it can be analytically continued to $s = 1$. We discuss the numerical evaluation of $Z_{00}^{\mathbf{d}}$ in section 5.2.

When we select the sector $\mathbf{d} = 0$, $\gamma = 1$, the formulae (18–19) become identical to eqs. (1.3–1.5) in ref. [13]. In this case, the channel $l = 2$ decouples from the $l = 0$ -channel, and it is sufficient to assume that phase shifts δ_4, $\delta_6,\ldots$ can be neglected. Because we are interested in the elastic two-particle scattering, the center of mass energy is restricted to the interval $2m_\phi < W_{\mathrm{CM}} < 4m_\phi$, or equivalently $0 < p^* < \sqrt{3}m_\phi$.

The function $\phi^{\mathbf{d}}$ is a function of 3 variables, q, γ and $\mathbf{d}$. In figure 2 we display $\phi^{\mathbf{d}}$ when $d = |\mathbf{d}| = 0$; $d = 1$ and $\gamma = 1$; and $d = 1$ and $\gamma = 1.1$. The points where $\phi^{\mathbf{d}}$ crosses levels $n\pi$ correspond to *free particle* energy levels; when $d = 0$ these occur at $q^2 = 0, 1, 2, 3,\ldots$, in accordance with eq. (12). The curve $d = 1$, $\gamma = 1$ is an artificial case and in effect neglects relativistic effects: in this case the momenta transform according to Galilean
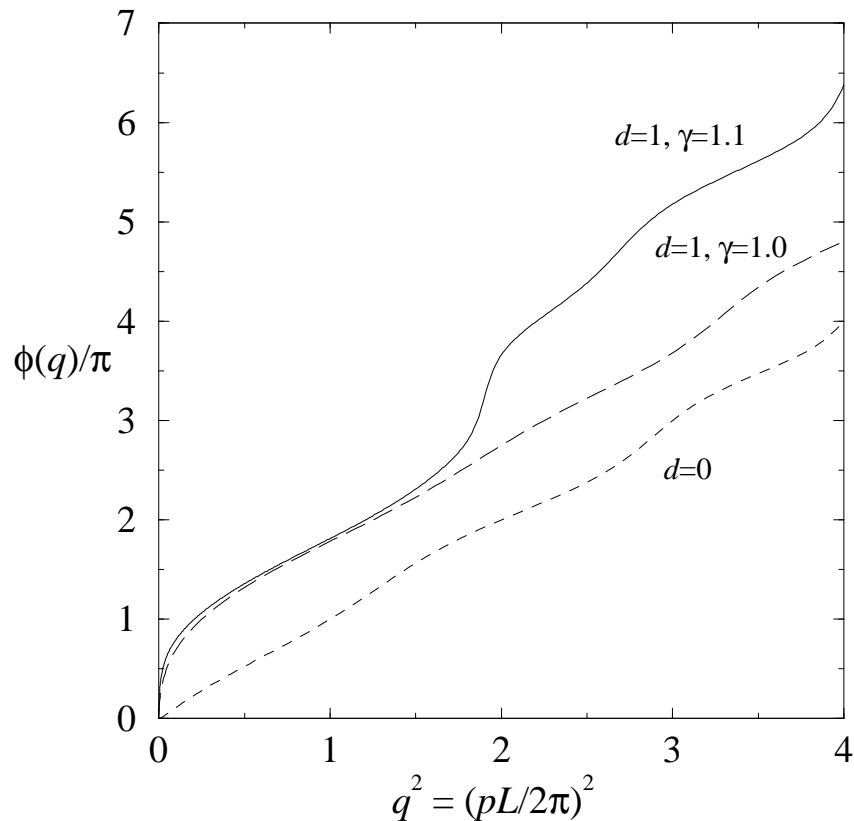
7

Figure 2: Function $\phi^{\mathbf{d}}(q)$. Dashed line is ϕ when the total momentum $\mathbf{P} = 0$ ($\mathbf{d} = 0$), line with long dashes with $\mathbf{P} = 2\pi/L$ and $\gamma = 0$, and solid line $\mathbf{P} = 2\pi/L$ and $\gamma = 1.1$.

transformations, and the free particle energy levels are at $q^2 = \frac{1}{4}, \frac{5}{4}, \frac{9}{4}, \ldots$. The third curve has $d = 1$ and γ has an arbitrary value of 1.1. As discussed above, the relativistic effects lift the degeneracy of some momentum states; this is evident by the rapid step-like cross-overs in the value of $\phi^{\mathbf{d}}$ by an amount of π at some values of q^2. When γ is decreased towards value 1 the breaking of the degeneracy becomes smaller, and the cross-overs of $\phi^{\mathbf{d}}$ approach a step function.

3   Monte Carlo simulations of the test model

To observe a resonance, we construct a model with a light mass field (ϕ) coupled to a field of heavier mass (ρ) with a 3-point coupling. The physical masses of the fields are in the elastic region $2m_\phi < m_\rho < 4m_\phi$. A computationally simple model with these features can be constructed by coupling two Ising fields with different masses. In two dimensions, this model has been successfully used by Gattringer and Lang to study the zero total

8

momentum resonance scattering [19]. With this model it is straightforward to adjust the masses of the particles and the strength of the coupling.

The Ising model is one representation of lattice ϕ^4 models. These models are most probably trivial and reduce to a free theory in the continuum limit. However, for small lattice spacings a and at energies substantially below the cutoff scale $1/a$ the model exhibits a well-defined scaling behavior, corresponding to an interacting continuum theory. In the scaling region the behavior of the ϕ^4 model is very well described with perturbative methods; this has been studied in detail both analytically [24] and with lattice Monte Carlo methods [25, 26].

3.1 Continuum action and perturbative phase shift

In Euclidean continuum formulation, the action of the model we consider in this work is

$$S = \int \mathrm{d}^4 x \left[\frac{1}{2}(\partial_\mu \phi)^2 + \frac{1}{2}m_{\pi,0}^2 \phi^2 + \frac{\lambda_0}{4!}\phi^4 + \frac{1}{2}(\partial_\mu \rho)^2 + \frac{1}{2}m_{\rho,0}^2 \rho^2 + \frac{\lambda_{\rho,0}}{4!}\rho^4 + \frac{g_0}{2}\rho\phi^2 \right] . \quad (21)$$

In practice, the coupling constant g is small enough that we expect the model to exhibit a scaling behavior similar to that of the ϕ^4 model. The parameters of the model are chosen so that the fields ϕ and ρ have physical masses in the elastic region $2m_\phi \leq m_\rho < 4m_\phi$.

The resonance scattering $\phi\phi \leftrightarrow \rho$ occurs through the $l = 0$ channel. The corresponding scattering phase shift δ_0 can be calculated perturbatively from action (21). At the resonance the partial amplitude becomes singular, and we can approximate the total phase shift as a sum of the singular contribution δ_s and the regular part δ_r:

$$\delta_0 = \delta_r + \delta_s \quad (22)$$

$$\delta_r = -\lambda_\mathrm{R}\frac{p}{16\pi W} + \frac{g_\mathrm{R}^2}{32\pi}\frac{1}{Wp}\log\frac{4p^2 + m_\rho^2}{m_\rho^2} \quad (23)$$

$$\tan\delta_s = -\frac{g_\mathrm{R}^2}{16\pi}\frac{p}{W}\frac{1}{W^2 - m_\rho^2} . \quad (24)$$

The masses m_ϕ and m_ρ are the physical masses of the particles, obtained from the real part of the propagator poles. The couplings λ_R and g_R are renormalized ϕ^4 and $\phi^2\rho$ coupling constants. The term proportional to λ_R in eq. (23) arises from the 4 point diagram. The g_R^2 terms come from the ρ particle interchanges; in eq. (23) from the sum of u and t channels and in eq. (24) from the s channel. The resonance width Γ_ρ is

$$\Gamma_\rho = \frac{g_\mathrm{R}^2}{32\pi m_\rho^2}\sqrt{m_\rho^2 - 4m_\phi^2} . \quad (25)$$

Besides the appearance of the λ_R term and different numerical factors, the formulae (22–24) are similar to the perturbative results in O(N) symmetric ϕ^4 theory in ref. [22].

3.2   Lattice action

Let us consider a lattice of size $L^3 \times T$ with periodic boundary conditions. For simplicity, we set the lattice spacing to unity, and an appropriate power of the lattice spacing is understood in all dimensionful quantities. The model is defined by the action

$$S = -\kappa_\phi \sum_{x;\hat{\mu}} \phi_x \phi_{x+\hat{\mu}} - \kappa_\rho \sum_{x;\hat{\mu}} \rho_x \rho_{x+\hat{\mu}} + g \sum_{x;\hat{\mu}} \rho_x \phi_x \phi_{x+\hat{\mu}} \,. \tag{26}$$

In the above summations x goes over the whole lattice and the vector $\hat{\mu} = \pm\mathbf{e}_\mu$, where $\mathbf{e}_\mu$ denotes a unit vector to direction μ. The field variables ϕ and ρ are restricted to values $\{-1, +1\}$. Since $\phi^2 = 1$, the 3-point term has been introduced in a nonlocal way. The hopping parameters κ_ϕ and κ_ρ are restricted to positive values, corresponding to ferromagnetic Ising coupling.

If the coupling constant $g = 0$, the model corresponds to two independent Ising models. In infinite volume, the 4-dimensional Ising model has a second order phase transition at $\kappa_\phi = \kappa_\rho \approx 0.074834(15)$ [27]. When $g \neq 0$, the third term in the action (26) gives rise to the interaction $\phi\phi \leftrightarrow \rho$, and by suitably choosing the couplings κ_ϕ and κ_ρ the ρ particle is rendered unstable. Since ρ is not an asymptotic state, its mass becomes ill-defined; in what follows we mean by the ρ mass m_ρ the energy level where the phase shift reaches the resonance value. Further, the action now preserves the symmetry $\phi \to -\phi$ but the symmetry $\rho \to -\rho$ is broken. This has implications for the phase structure of the model. Let us discuss the case where all coupling constants are greater than 0 but finite. When g is small enough, the effective hopping parameter for the ϕ field becomes local, but it remains still positive: $\kappa_{\text{eff}}(x, \mu) = \kappa_\phi - \frac{1}{2}g(\rho_x + \rho_{x+\hat{\mu}}) > 0$. For a fixed ρ configuration, the action of the ϕ field corresponds to a ferromagnetic spin glass, which still has an Ising-like second order phase transition between phases where $\langle\phi\rangle = 0$ and $\langle\phi\rangle \neq 0$ in the thermodynamic limit ($L, T \to \infty$). It is not known to us whether this transition survives the dynamic ρ field. However, this seems plausible, since the expectation value of ϕ is still driven to zero when κ_ϕ is small enough (but still > 0) and acquires a non-zero value with large enough κ_ϕ.

When $\kappa_\phi > g$ the expectation value $\langle\phi_x\phi_{x+\hat{\mu}}\rangle > 0$, and the third term of the action (26) acts like a biased random magnetic field on the ρ-configuration. The expectation value of ρ remains non-zero at all finite values of the hopping parameter κ_ρ, and hence the Ising phase transition of the ρ field disappears. Thus, for any fixed κ_ρ there is probably an upper limit on the (disconnected) correlation length of the ρ field, corresponding to a lower limit on m_ρ in lattice units. m_ρ can be made smaller only by simultaneously tuning κ_ρ and g.

The model described by the action (26) is most probably trivial like the Ising model, and it does not have a continuum limit. However, with small but finite lattice spacing the model effectively describes an interacting continuum field theory. For our purposes this is sufficient, since our main interest is in the technical methods for extracting the scattering

phase shift from an interacting effective theory. However, this makes the analysis of the effects caused by the finite lattice spacing by the standard method of performing simulations with several different lattice spacings difficult: models with different lattice spacings (correlation lengths) correspond to different continuum theories.

3.2.1 Update algorithm

The spins are updated with a 4-dimensional analogue of the cluster algorithm already used in 2-dimensional simulations [19]. The ϕ and ρ-spins are updated in separate cluster update sweeps using modified Swendsen-Wang [28] type percolation cluster algorithms.

In the ϕ update the clusters are grown using the local hopping parameter $\kappa_{\text{eff}}(x, \mu) = \kappa_\phi - \frac{1}{2}g(\rho_x + \rho_{x+\hat{\mu}})$. The link from point x to point $x + \hat{\mu}$ is *activated* with the probability $(1 - e^{-2\kappa_{\text{eff}}(x,\mu)})\,\delta(\phi_x, \phi_{x+\hat{\mu}})$. The clusters are grown over the activated links with the Hoshen-Kopelman algorithm [29]. After all the clusters are formed, all of the spins in each cluster are set to value $+1$ or -1 with equal probabilities.

In the update of the ρ field the links are activated with probability $(1 - e^{-2\kappa_\rho})\,\delta(\rho_x, \rho_{x+\hat{\mu}})$. After the clusters are formed, we calculate the net external field induced by the ϕ field acting on the cluster C, and the spins in C are set to value $+1$ with probability

$$p_+ = \left(1 + \exp[g \sum_{x \in C; \mu} \phi_x(\phi_{x+\hat{\mu}} + \phi_{x-\hat{\mu}})]\right)^{-1}. \tag{27}$$

The probability of setting the spins in cluster C to -1 is $p_- = 1 - p_+$.

For our choices of the run parameters the cluster update is a clear improvement over the local Metropolis algorithm, especially for the ϕ field, which has longer correlation length. For the ρ field update the difference between the local and cluster update is smaller, but still appreciable.

3.3   The simulation parameters

In order to achieve the resonating behavior the couplings in the action (26) have to be tuned so that the ρ resonance lies in the elastic region: $2m_\phi < m_\rho < 4m_\phi$. For each (fixed) coupling g, we adjust the hopping parameters κ_ϕ and κ_ρ so that the ϕ field is in the symmetric phase ($\langle\phi\rangle = 0$) and the above inequalities hold. The hopping parameters were tuned by performing simulations with small lattices and measuring the single particle correlation lengths for ϕ and ρ fields (the resonance turns out to be so narrow that the single particle correlation length yields a very good estimate of the resonance mass for practical lattice sizes).

The production runs were performed with 3 different sets of the coupling constants, and the values of the couplings are listed in table 1. The parameter sets are labelled with symbols A, B and C. In case A we set the coupling constant $g = 0$ to test the

	A	B	C
κ_ϕ	0.0742	0.07325	0.07075
κ_ρ	0.0708	0.0718	0.0665
g	0	0.008	0.021
# of lattice sizes	9	10	16
$m_\phi\, a$	0.1856(4)	0.1996(5)	0.3081(4)
$m_\rho\, a$	0.5049(5)	0.5306(13)	0.8206(11)
$\Gamma_\rho\, a$	0	0.0044(2)	0.0178(7)
$g_{\rm R}\, a$	0	0.598(14)	1.49(3)
$\lambda_{\rm R}$	28.1(1.1)	36.8(1.3)	48.3(2.0)

Table 1: Compilation of the run parameters and results of the mass and resonance parameter measurements.

calculational methods in the absence of the 3 point coupling; B and C have $g = 0.008$ and 0.021, respectively. Sets A and B correspond roughly to masses $m_\phi a \sim 0.2$ and $m_\rho a \sim 0.5$; however, no special attempt was made to tune the masses very precisely. In the case C we set $m_\phi a \sim 0.3$ and $m_\rho a \sim 0.8$ in order to be able to use smaller lattice volumes and save computation time. Even in this case the finite lattice spacing effects turn out to be well in control (sect. 3.4).

The sets A, B and C consist of 9, 10 and 16 different lattice sizes, respectively. The size of the largest lattice in each of the sets is $36^3 \times 40$. In all of the lattices the time extent T was larger than the spatial lattice length L.

The Monte Carlo simulations consisted of $30\,000 - 65\,000$ cluster update sweeps for both of the spins for each lattice. The correlation function measurements, described in sections 3.4 and 3.5, were performed after every 2 full update sweeps, and 500 consecutive measurements were blocked together. The final error analysis was done by applying the jackknife method to the blocked data. At the end, we had $30 - 65$ jackknife blocks for each lattice. In what follows, the cited error bars are all only statistical one standard deviation errors. The data collected are quite sufficient for measuring the correlation functions to the accuracy needed in order to extract the phase shift. Only for the largest volumes does the statistical noise start to affect the signal to any large extent. The simulations were performed on IBM RS/6000, DEC Alpha and Sun workstations, and the total CPU time used was approximately 1800 hours.
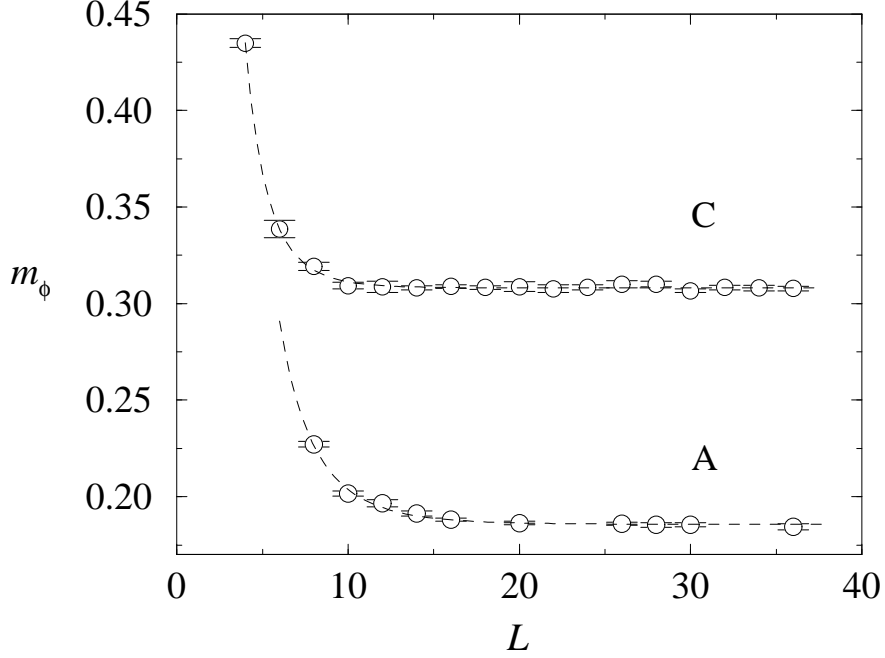
Figure 3: The finite size dependence of the mass of the ϕ field for coupling constant sets A (bottom) and C (top). The results of the fits of function (30) are shown with dashed lines.

3.4 Single particle spectrum and lattice effects

In order to calculate the phase shift, we need an accurate determination of the single particle mass of ϕ field m_ϕ. The single particle energy spectrum gives also an estimate of the finite lattice spacing and finite volume effects. These effects are expected to be small provided $m_\phi L \gg 1$ and $|\mathbf{p}| \ll 1$.

In order to measure the correlations, we take the spatial Fourier transform of the field ϕ:

$$\widetilde{\phi}(\mathbf{n}, t) = \frac{1}{L^3} \sum_{\mathbf{x}} \phi(\mathbf{x}, t) e^{i\mathbf{x} \cdot \mathbf{p}} \tag{28}$$

where $\mathbf{p} = (2\pi/L)\mathbf{n}$, and $-L/2 + 1 \le n_i \le L/2$. The single particle energy spectrum can be extracted from the exponential decay of the correlation functions

$$C_i(t) = \left\langle \sum_{\mathbf{n};\, \mathbf{n}^2 = i} \widetilde{\phi}(-\mathbf{n}, t)\widetilde{\phi}(\mathbf{n}, 0) \right\rangle \propto e^{-E(\mathbf{p})t}. \tag{29}$$

For each lattice, we measure 5 ϕ field correlation functions $C_0 - C_4$, corresponding to momenta $\mathbf{p}L/(2\pi) = (0,0,0)$, (1,0,0), (1,1,0), (1,1,1), (2,0,0) and permutations.

13

The single particle mass is extracted from the zero momentum correlation function $C_0(t) \sim e^{-m_\phi(L)t}$. We expect that the finite volume polarization – the self-interactions of the field around the periodic torus – affects the mass as

$$m_\phi(L) = m_\phi + c\, L^{-3/2}\, e^{-m_\phi L} \,, \tag{30}$$

with a constant c. The infinite volume mass m_ϕ is obtained by fitting the function (30) to the measured mass values $m_\phi(L)$. The result of the fits are given in table 1, with one standard deviation errors. In figure 3 we show the data and the fitted function for cases A and C; case B is very similar to case A. In case C, the finite size effects practically disappear into the statistical noise when $L \geq 12$.

In order to study the effects of the finite lattice spacing, we compare the non zero momentum single particle energy levels to the continuum relation

$$E(\mathbf{p}) = \sqrt{\mathbf{p}^2 + m_\phi^2} \tag{31}$$

and to the lattice dispersion relation, valid for Gaussian fields on the lattice

$$\cosh E(\mathbf{p}) - \cosh m_\phi = \sum_{i=1}^{3}(1 - \cos p_i). \tag{32}$$

In figure 4 we display the measured values of $E(p)$ and the continuum and lattice dispersion relations, eqs. (31) and (32), for 3 lattices belonging to series A. The continuum dispersion relation is clearly insufficient, and diverges from the measured dispersion $\sim p^2$. On the other hand, the lattice dispersion relation fits the measured energies strikingly well – in the bottom part of figure 4 the difference between the data and the lattice dispersion can be completely attributed to statistical errors. The other lattice volumes and cases B and C behave in a qualitatively similar fashion. It should be noted that the lattice dispersion relation (32) is defined only at discrete momenta $p_i = (2\pi/L)n_i$, $n_i \in \mathbf{Z}$.

In case A, the ρ particle is stable, and we can check the finite size and the finite lattice spacing effects on ρ energy levels. The mass spectrum is measured with analogous operators to eq. (28), but we only measure momentum states $p = 0$ and $p = 2\pi/L$. In the zero momentum case, we do not find any appreciable finite size effects, and the value of m_ρ given in table 1 is an average over all lattices. The non zero momentum energy levels are shown in figure 4. They also deviate from the continuum dispersion relation, but are well described by the lattice dispersion.

The finite lattice spacing effects are large enough that we cannot use the continuum dispersion relation when we determine the scattering phase shifts. However, the use of the lattice dispersion relation (32) can be problematic, since the momenta in this case are not restricted to "lattice momenta" $\mathbf{n}2\pi/L$ any more. This is discussed further in section 3.5.
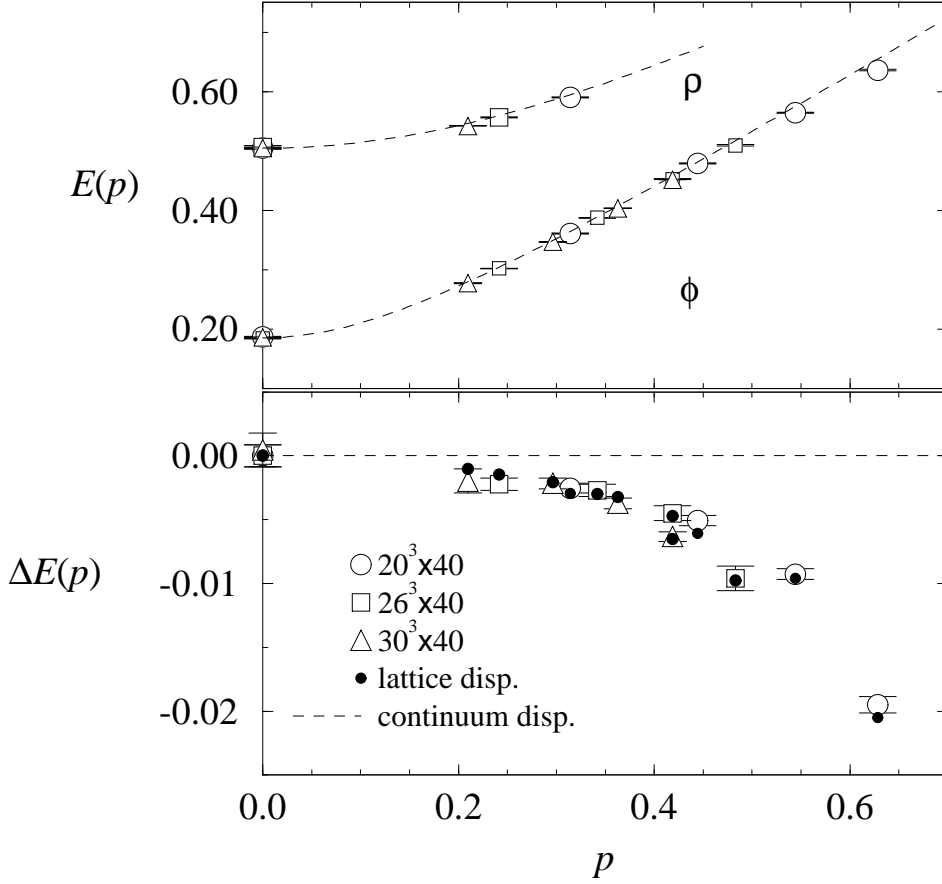
14

Figure 4: The single particle energy levels of case A lattices of spatial size 20^3, 26^3 and 30^3. Top: the measured energy levels together with the continuum dispersion relation, eq. (31) (dashed line) for ϕ and ρ. Bottom: the measured ϕ energy levels and the lattice dispersion relation eq. (32) (black dots); here the continuum dispersion relation has been subtracted to emphasize the difference.

3.5   Two-particle spectrum

To measure the two-particle energy levels we need operators of type

$$\mathcal{O}_{\mathbf{d},\mathbf{n}}(t) = \widetilde{\phi}(\mathbf{n} + \mathbf{d}, t)\widetilde{\phi}(-\mathbf{n}, t) \tag{33}$$

where $\widetilde{\phi}$ is the spatial Fourier transform of the ϕ field, defined in eq. (28), and $\mathbf{d}\,,\mathbf{n} \in \mathbf{Z}^3$. This operator describes two ϕ particles with total 3-momentum $\mathbf{P} = (2\pi/L)\,\mathbf{d}$. For each value of vector $\mathbf{d}$ the operators (33) form a complete basis for two ϕ particles. The energy eigenstates can be constructed as linear combinations of these operators and the ρ operator belonging to the same total momentum sector. On an L^3 spatial lattice there are

15

L^3 different operators of type (33) for each value of $\mathbf{d}$; however, it turns out that only a few lowest momentum operators are needed. The energy eigenstates are measured as follows: first, we pick a suitable set of operators $\mathcal{O}_\alpha$, measure a matrix of correlation functions $\langle \mathcal{O}_\alpha^\dagger(t)\mathcal{O}_\beta(0)\rangle$, and diagonalize the matrix. The energy eigenvalues can be extracted from the exponential decay of the eigenvalues of the correlation function matrix.

To construct the operators (33) we first form the Fourier transforms of the field ϕ for momenta $\mathbf{p}L/(2\pi) = (0,0,0)$, (1,0,0), (1,1,0), (1,1,1), (2,0,0), and non-equivalent permutations and signs, all in all 17 functions. (Note that because the field is real there is no need for separate computation of $-\mathbf{p}$ and $\mathbf{p}$.) In the $\mathbf{P} = 0$ sector, these are combined into 5 different operators

$$O_{0,i}(t) = \frac{1}{N_i} \sum_{\mathbf{n}} \delta_{\mathbf{n}^2,i-1}\, \widetilde{\phi}(\mathbf{n},t)\widetilde{\phi}(-\mathbf{n},t) \qquad i = 1,2,3,4,5\,, \tag{34}$$

where $N_i = \sum_{\mathbf{n}} \delta_{\mathbf{n}^2,i-1}$. In the $d = |\mathbf{d}| = 1$ sector we have 4 operators for each of the 3 directions of $\mathbf{d}$. For concreteness, let $\mathbf{d} = \mathbf{e}_3$; now the operators are

$$
\begin{aligned}
O_{\mathbf{e}_3,1}(t) &= \widetilde{\phi}(\mathbf{e}_3,t)\widetilde{\phi}(0,t) \\
O_{\mathbf{e}_3,2}(t) &= \frac{1}{4}\sum_{\mathbf{n}} \delta_{n_3,0}\,\delta_{n^2,1}\, \widetilde{\phi}(\mathbf{n}+\mathbf{e}_3,t)\widetilde{\phi}(-\mathbf{n},t) \\
O_{\mathbf{e}_3,3}(t) &= \widetilde{\phi}(2\mathbf{e}_3,t)\widetilde{\phi}(-\mathbf{e}_3,t) \\
O_{\mathbf{e}_3,4}(t) &= \frac{1}{4}\sum_{\mathbf{n}} \delta_{n_3,0}\,\delta_{n^2,2}\, \widetilde{\phi}(\mathbf{n}+\mathbf{e}_3,t)\widetilde{\phi}(-\mathbf{n},t)\,.
\end{aligned}
\tag{35}
$$

The ordering of the operator is such that the free particle energy levels increase with increasing operator numbers. The summation over $\mathbf{n}$ in the above operators makes them cubically ($d = 0$) and tetragonally ($d = 1$) invariant. This enhances their coupling to the states which belong to the A_1^+ representation of the cubic and tetragonal groups (see section 5.1 for details).

Let us now define the ρ field operator $O_{\mathbf{d},0}(t) = \widetilde{\rho}(\mathbf{d},t)$, where $|\mathbf{d}| = 0$ or 1. With these operators we measure the correlation function matrices

$$
\begin{aligned}
C^0_{\alpha\beta}(t) &= \langle O_{0,\alpha}(t)\,O_{0,\beta}(0)\rangle_c & (36) \\
C^1_{\alpha\beta}(t) &= \frac{1}{3}\sum_{i=1,2,3} \left\langle O^*_{\mathbf{e}_i,\alpha}(t)\,O_{\mathbf{e}_i,\beta}(0)\right\rangle_c & (37)
\end{aligned}
$$

where $\alpha, \beta = 0,1,2,\ldots$, and $\langle\cdot\rangle_c$ denotes the connected part of the correlation function. Both of the matrices are real and symmetric; $C^0_{\alpha\beta}$ by construction and $C^1_{\alpha\beta}$ by statistical averaging (which can be made explicit with the relation $O_{\mathbf{e},\alpha} = O^*_{-\mathbf{e},\alpha}$).

The correlation functions entering the matrix $C^1_{\alpha\beta}$ have vanishing disconnected contributions. The disconnected part of the correlations in the matrix $C^0_{\alpha\beta}$ can be excluded by

16

considering instead of the function (36) the correlation function [18]

$$C^0_{\alpha\beta}(t) = \langle [O_{0,\alpha}(t) - O_{0,\alpha}(t+1)] O_{0,\beta}(0) \rangle . \tag{38}$$

The spectral decomposition of the matrices C^0 and C^1 has the form

$$C^d_{\alpha\beta} = \sum_a v^{d,a*}_\alpha v^{d,a}_\beta e^{-tW^d_a} \qquad v^{d,a}_\alpha = c^d_a \langle a|O^d_\alpha(0)|0 \rangle , \tag{39}$$

where a labels the energy eigenstates (of energy W^d_a), d is either 0 or 1, and the coefficient $c^0_a = (1 - e^{-W^0_a})^{1/2}$ and $c^1_a = 1$.

The energies W^d_a can now be solved from the eigenvalue equation $C^d(t)\psi^d_a = \lambda^d_a(t)\psi^d_a$, where we expect $\lambda^d_a(t) \sim e^{-tW^d_a}$ when t is large enough. However, the signal becomes exponentially smaller when t increases, and is soon lost into statistical noise. The better the set of operators used in the C-matrices spans the space of the lowest energy eigenstates, the faster the convergence is. The number of operators should be larger than the number of energy eigenstates in the elastic regime $2m_\phi \leq W < 4m_\phi$. A larger set provides a better representation of the eigenstates at the expense of increased numerical noise.

Lüscher and Wolff [18] proposed a method that allows a reliable determination of the energy levels even at small values of t. Let us define the generalized eigenvalue problem (we drop the label d in the following formulae; they are valid for both $d = 0$ and $d = 1$)

$$C(t)\psi_a = \lambda_a(t, t_0) C(t_0)\psi_a \tag{40}$$

where t_0 is a small reference time ($t_0 = 0$, for example). The eigenvalues are given by

$$\lambda_a(t, t_0) = e^{-(t-t_0)W_a} \tag{41}$$

up to negligible corrections exponential in $t - t_0$. Note that $\lambda_a(t_0, t_0) = 1$ by construction. This method can be implemented by studying the (standard) eigenvalue problem of matrices

$$D(t) = C^{-1/2}(t_0)C(t)C^{-1/2}(t_0) \tag{42}$$

which has eigenvalues $\lambda_a(t, t_0)$ and eigenvectors $\Psi_a = C^{1/2}(t_0)\psi_a$.

In our simulations we always measure the 6×6 ($d = 0$) and 5×5 ($d = 1$) matrices as defined in eqs. (38) and (37). In the case of smallest volumes ($L \leq 10$–12) we drop the highest momentum correlation functions before analyzing the eigenvalues. For the largest volumes, there are more states below elastic threshold than the dimension of the matrices; nevertheless, we could always find the lowest 3–4 eigenstates without problems.

3.6   Energy spectrum

We measure the correlation function matrices $C^0(t)_{\alpha\beta}$ and $C^1(t)_{\alpha\beta}$, eqs. (38) and (37), up to the distance $T/2$; all the measurements are blocked into $35 - 65$ blocks, which are

used as independent measurements for jackknife error analysis. To obtain the transformed correlation matrix $D(t) = C^{-1/2}(t_0)C(t)C^{-1/2}(t_0)$ we choose the reference time $t_0 = 0$; in our checks the results were virtually unchanged for other (small) choices of t_0.

We diagonalize the matrices $D(t)$ and order the eigenvalues $\lambda_a(t)$, $t > 0$, so that $\lambda_1 > \lambda_2 > \ldots > \lambda_n$. The energy spectrum is determined by a fully correlated one-parameter exponential fit $\lambda_a(t) = \exp(-W_a t)$. The fit range varies from $t = 0$–10 to 0–4; the end point of the range is adjusted until an acceptable χ^2 per degree of freedom is obtained. Generally, the length of the range can be chosen longer with lower energy states and larger lattices. The effect of using fit functions of correct periodicity has a negligible effect on the energy spectrum (for correlations $D^0(t)$ the correct form is $\propto \exp[-W_a t] - \exp[-W_a(L - t - 1)]$, due to the definition eq. (38); for correlations $D^1(t)$ it is $\propto \exp[-W_a t] + \exp[-W_a(L - t)]$).

When the total momentum $\mathbf{P} = 2\pi\mathbf{e}_i/L$ the eigenvalue analysis yields only the laboratory frame energies $W_{\mathrm{L},a}$. These have to be transformed into the center of mass frame. In the continuum, the relation between the center of mass and laboratory frame energies is given by

$$W_{\mathrm{CM},a} = \sqrt{W_{\mathrm{L},a}^2 - P^2} \tag{43}$$

(see eq. (13)). However, this relation is affected by the finite lattice spacing, and motivated by the lattice dispersion relation (32) we define

$$\cosh W_{\mathrm{CM},a} = \cosh W_{\mathrm{L},a} - (1 - \cos P). \tag{44}$$

The use of this relation is also justified by the excellent agreement between the results of $P = 0$ and $P = 2\pi/L$ when the phase shift function is determined (section 3.7); if the relation (43) is used instead, there remains a clear systematic difference between the momentum sectors.

The center of mass energy levels are shown in figures 5, 6 and 7 for cases A, B and C, respectively, and for both momentum sectors $P = 0$ and $P = 2\pi/L$ (left and right figures). The energy level $W = 2m_\phi$ and the inelastic threshold $W = 4m_\phi$ are shown with horizontal dotted lines.[2] Above the inelastic limit new 4 particle states appear and our analysis loses its validity (it should be noted that the 3 particle states do not couple to the 2 particle ones due to the lack of the ϕ^3 coupling).

The solid lines in figures 5–7 are perturbative energy levels determined by fitting equations (22–24) to the phase shift data. In all cases the consistency of the fits is excellent, although the χ^2 values are not necessarily very good. The extraction of the phase shift data and the fitting procedure are described in section 3.7.

---

[2]In the $P = 2\pi/L$ case, the inelastic limit is actually *greater* than $4m_\phi$: when we ignore the interactions, in the laboratory frame the threshold is $W_{\mathrm{L,inel.}} = 3m_\phi + [m_\phi^2 + (2\pi/L)^2]^{1/2}$, corresponding to 3 particles at rest and one moving with momentum $p = 2\pi/L$. In the cm-frame this yields $W_{\mathrm{CM,inel.}}^2 = 10m_\phi^2 + 6m_\phi[m_\phi^2 + (2\pi/L)^2]^{1/2} > (4m_\phi)^2$.
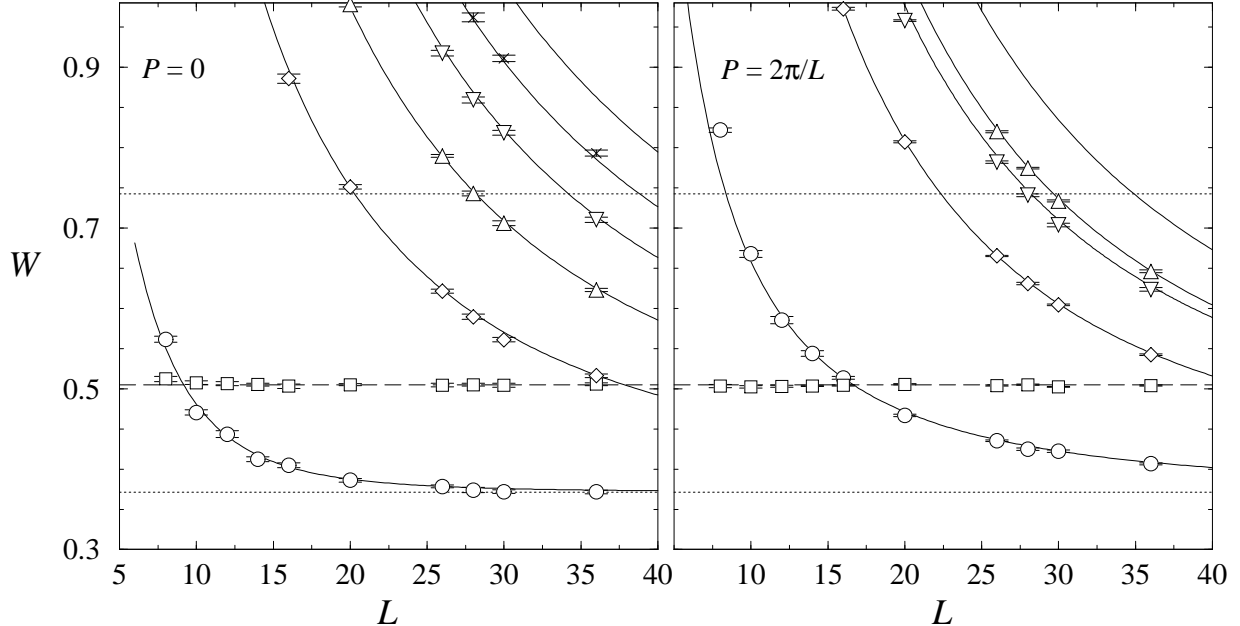
Figure 5: The center of mass frame energy levels for case A ($g = 0$) for $P = 0$ and $P = 2\pi/L$. The horizontal dotted lines show the energy levels $2m_\phi$ and $4m_\phi$, and the dashed line corresponds to $W = m_\rho$. The continuous curves are perturbative energy levels fitted to the phase shift function (sec. 3.7).

In case A the $\phi^2\rho$ coupling is absent and the ρ particle is stable. The energy level $W = m_\rho$ is shown with a horizontal dashed line in fig. 5. In cases B and C m_ρ is determined by the fit to the perturbative ansatz eq. (24) and shown in figs. 6 and 7 with dashed lines.

Qualitatively, the essential difference between the non-resonance case (A) and the resonating cases (B and C) is obvious: the intersections of the 2ϕ levels with the ρ energy level in case A turn into avoided level crossings in cases B and C. It is especially illuminating to consider cases A and B, which correspond to nearly identical values of m_ϕ and m_ρ: when the total momentum $P = 0$, the lowest level crossing occurs at $L \sim 9$. This level crossing, absent in the free theory (see fig. 1), is caused by the repulsive $\lambda\phi^4$ interaction which increases the energy of the lowest 2 particle state. If $\lambda < 0$, the energy of the lowest state decreases with decreasing lattice size, and the first level crossing vanishes (This effectively occurs in O(4)-symmetric ϕ^4 theory in external field [22]).

In the $P = 2\pi/L$ sector the first (avoided) level crossing has moved up to $L \sim 16$. This crossing is determined by the kinematics of the ϕ and ρ particles, and it persists irrespective of the value of λ. In our case this is the first "useful" level crossing, since the first crossing in the $P = 0$ sector occurs at such a small volume ($L < 2m_\phi^{-1}$) that the reliability is compromised by the finite volume polarization effects (nevertheless, to
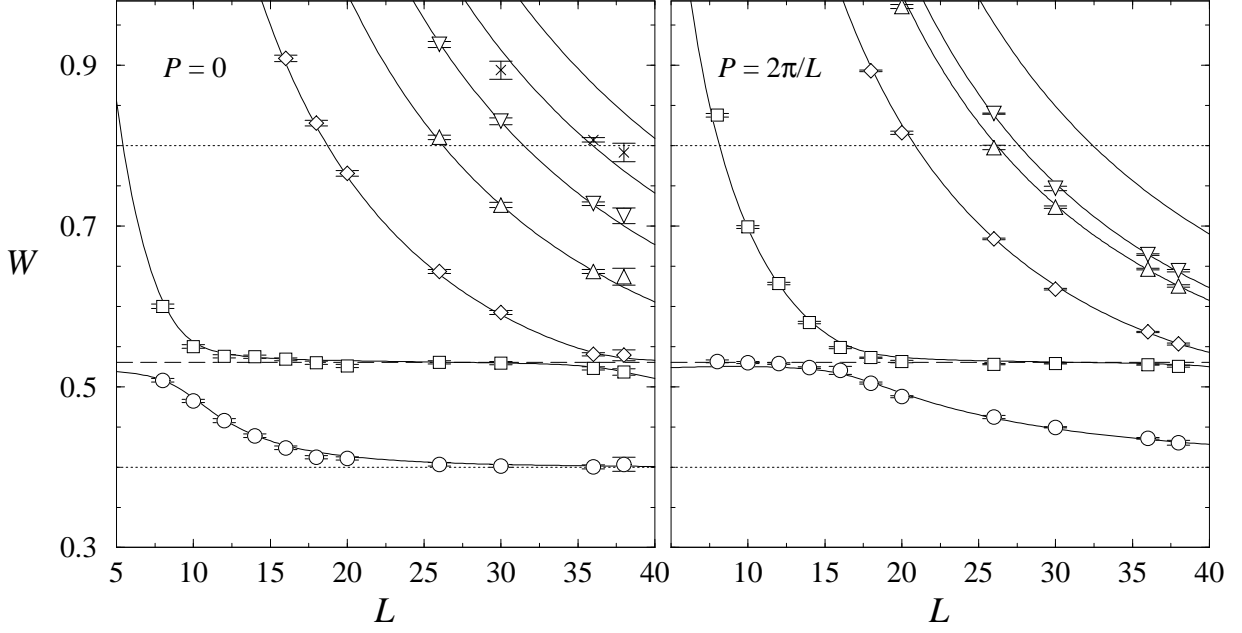
Figure 6: The center of mass frame energy levels for case B ($g = 0.008$). The resonance mass m_ρ is shown with a dashed line, levels $W = 2m_\phi$ and $4m_\phi$ with dotted lines, and the perturbative fit with continuous lines.
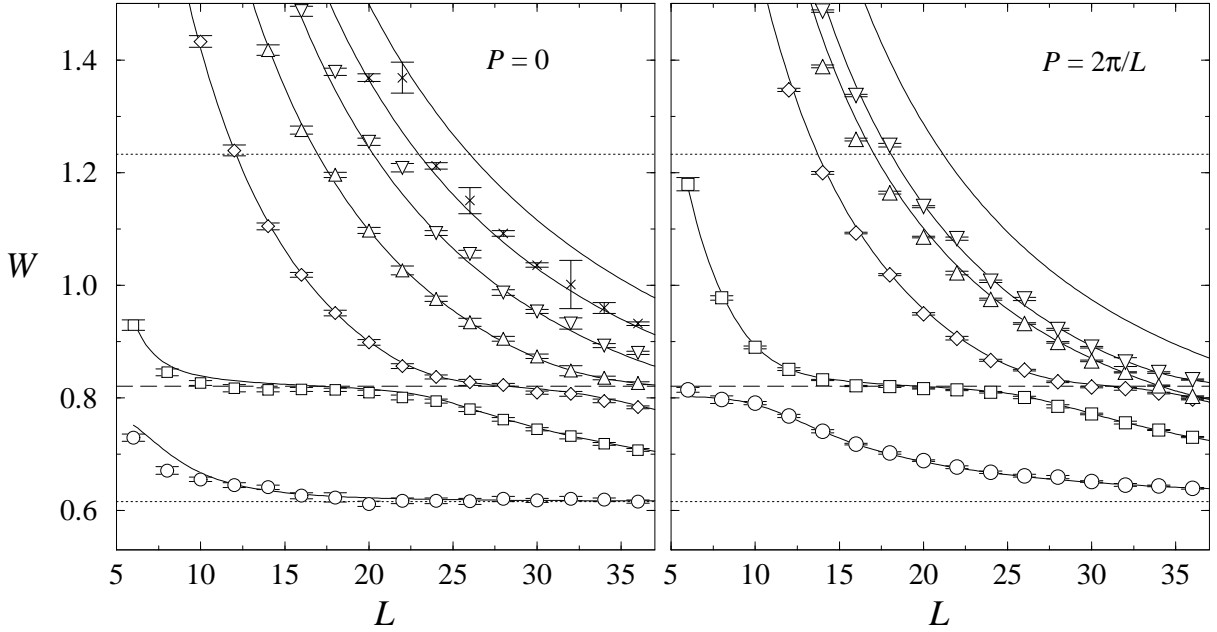

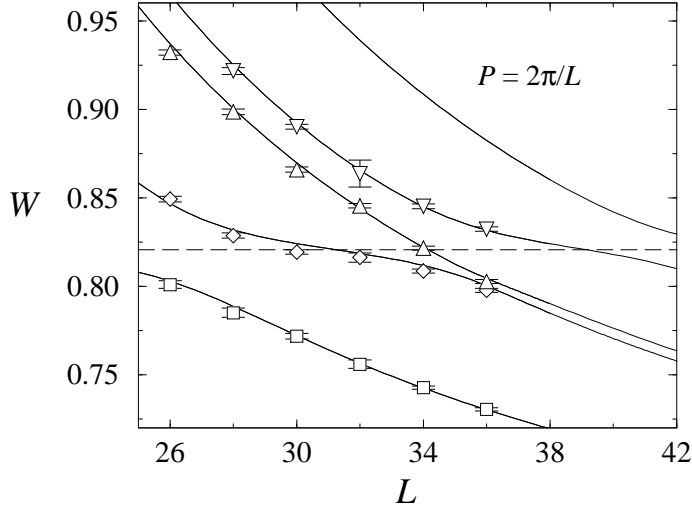Figure 7: The center of mass frame energy levels for case C ($g = 0.021$).

Figure 8: Close-up of the $P = 2\pi/L$ sector energy levels in case C. The energy levels shown are numbers 2 (box), 3 (diamond), 4 (triangle up) and 5 (triangle down), counted from the lowest energy state up.

our surprise the data and the perturbative fits agree quite well even down to the smallest volumes — which were not used to determine the fit).

In case C the parameters were chosen so that the values of m_ϕ and m_ρ are $\sim 50\%$ larger than in A and B. This allows us to observe 3 avoided level crossings in the range $L = 6$–36 as opposed to 2 in case B. The coupling constant g is also considerably larger (0.021 vs. 0.008), giving a broader resonance.

We also observe the appearance of the closely spaced energy levels (numbers 4 and 5 from the lowest up) in the $P = 2\pi/L$ case. In the free theory these correspond to the laboratory frame momentum states $\mathbf{q}_1 = (0,0,2)$, $\mathbf{q}_2 = (0,0,-1)$ and $\mathbf{q}_1 = (1,1,1)$, $\mathbf{q}_2 = (0,-1,-1)$, respectively (here $\mathbf{q}_i = \mathbf{p}_i \, 2\pi/L$); the degeneracy of these states is lifted by relativistic effects (see the discussion in section 2.1).

In case C the largest volume is just large enough so that the $P = 2\pi/L$ levels 4 and 5 are in the middle of the avoided level crossing region. A close-up view of this region is shown in figure 8. At volumes smaller than $\sim 34^3$ the levels 4 and 5 are close to each other, and at larger volumes the levels 3 and 4 are nearly degenerate. Even in this complicated region the agreement between the data and the perturbative fit is remarkable, especially since none of the data of the levels 3, 4 and 5 is used to determine the fit parameters.

Generally, the statistical errors in the $P = 2\pi/L$ sector tend to be smaller than in the $P = 0$ sector. This is probably due to two reasons: the correlation functions in the $P = 2\pi/L$ sector do not have a disconnected part which needs to be subtracted (cf. equations (38) and (37)), and the statistics is increased by combining the measurements in $\mathbf{P} =$

$2\pi\mathbf{e}_i/L$, $i = 1, 2, 3$ sectors together. While not being completely statistically independent — the operators with different directions of $\mathbf{P}$ still act on the same configurations — the operators belonging to different sectors are orthogonal; i.e.,the cross-correlations between operators belonging in different $\mathbf{P} = 2\pi\mathbf{e}_i/L$ sectors vanish.

3.7 Scattering phase shift

In order to calculate the phase shift $\delta_0(p)$ from the fundamental equations (17–19), we need to transform the energy eigenvalues W_a to the corresponding momenta p_a. In continuum, the relation is given by eq. (4): $p_a^2 = (W_a/2)^2 - m_\phi^2$. However, as was observed in the analysis of the single particle energy spectrum in section 3.4, the lattice dispersion relation

$$\cosh\frac{W_a}{2} - \cosh m_\phi = \sum_{i=1}^{3}(1 - \cos p_{a,i}) \tag{45}$$

can be expected to give a much more accurate relation when the lattice spacing is finite. However, due to the breaking of the translational and rotational symmetries on the lattice the assignment $W_a \to p_a(W_a)$ is not uniquely defined by eq. (45). This problem can be circumvented by various approximations: since we are interested in the elastic region $0 \le p_a < \sqrt{3}m_\phi$, the magnitude of p_a is rather small (in lattice units) and it is bracketed by

$$\sqrt{3}\cos^{-1}(1 - \frac{1}{3}x) \le p_a \le \cos^{-1}(1 - x) \tag{46}$$

where $x \equiv \cosh(W_a/2) - \cosh m_\phi$. The first limit is saturated when $p_1 = p_2 = p_3 = p/\sqrt{3}$, and the second when $p_1 = p$, $p_2 = p_3 = 0$. The difference is maximal at the inelastic limit $W_a = 4m_\phi$, and using $m_\phi = 0.3$ ($\sim$ our largest value, case C) the limits become $0.5315 \le p_a(4m_\phi) \le 0.5358$: the uncertainty in p_a is always smaller than one percent, and in the important region $W_a \sim m_\rho$ it is still smaller. Either of the limits above can be used to calculate $p_a(W_a)$; however, the statistical quality of the data is good enough that the results are not compatible (i.e.,not within one standard deviation of each other).

We refine the estimate of p_a as follows: we find two consecutive *free particle* energy levels W_n and W_{n+1} so that $W_n \le W_a \le W_{n+1}$. These energy levels are calculated from the lattice dispersion relation (45) using lattice momenta $\mathbf{p} = (2\pi/L)\mathbf{m}$ in the $P = 0$ sector and $\mathbf{p} = (2\pi/L)\vec{\gamma}(\mathbf{m} + \mathbf{e}_3/2)$ in the $\mathbf{P} = 2\pi\mathbf{e}_3/L$ sector[3] ($\mathbf{m} \in \mathbf{Z}^3$). The desired momentum vector $\mathbf{p}_a$ is then found by interpolating $\mathbf{p}_a = r\mathbf{p}_n + (1 - r)\mathbf{p}_{n+1}$, $0 \le r \le 1$, until eq. (45) is satisfied. This method presupposes that the eigenstates with energies in between two free levels predominantly consist of a mixture of the two free states. This is supported by the analysis of the eigenvectors at the end of this section.

---

[3]The value of γ in the $P = 2\pi/L$ sector is calculated from $\gamma = W_{\mathrm{L}}/W_{\mathrm{CM}}$; see eqs. (6–9).
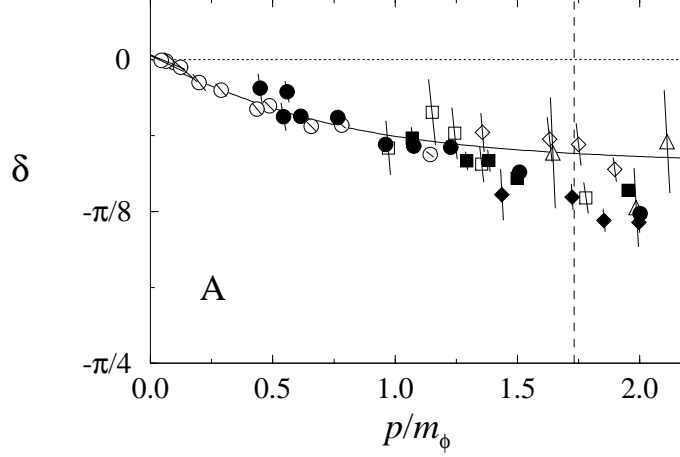
Figure 9: The phase shift for case A ($g = 0$). Open and filled symbols belong to sectors $P = 0$ and $P = 2\pi/L$, respectively. The inelastic limit $p = \sqrt{3}m_\phi$ is shown with a vertical dashed line, and the solid line is a perturbative fit.
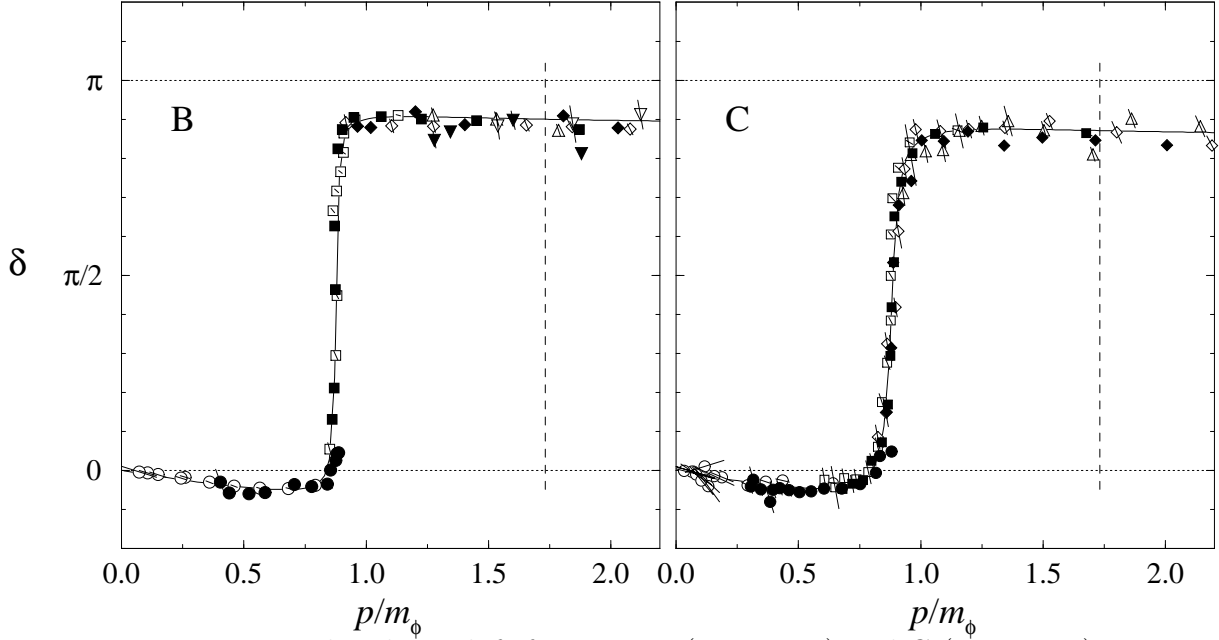
Figure 10: The phase shift for cases B ($g = 0.008$) and C ($g = 0.021$).

The phase shift is calculated by inserting the momenta p_a to eqs. (17–19). In figure 9 we show the phase shift of case A as a function of the center of mass momentum for both $P = 0$ and $P = 2\pi/L$ sectors with open and filled symbols, respectively. The tilted lines are one standard deviation errors; since p_a completely determines δ_0 by eq. (17) the errors in the values of p_a and δ_0 are fully correlated.

23

The phase shifts of cases B and C are shown in figure 10. The emergence of the resonance is evidenced by the rapid increase in δ_0 by π when $p^2 + m_\phi^2 \approx (m_\rho/2)^2$ (Note the difference in the vertical scales in figures 9 and 10). In figures 9 and 10 the symbol shapes are the same as in the energy level figures 5–7.

The consistency between the two total momentum sectors is good in all three cases. However, one can observe some systematic differences between the phase shift calculated from the data from different energy levels, especially at large momenta ($p \sim p_{\text{inelastic}}$). This is likely due to some unaccounted for lattice effects.

3.7.1 Resonance parameters

The tree level perturbative calculation gives the scattering phase shift in the $l = 0$ sector as $\delta_0(p) = \delta_r(p) + \delta_s(p)$, where

$$\delta_r = -\lambda_{\text{R}} \frac{p}{16\pi W} + \frac{g_{\text{R}}^2}{32\pi} \frac{1}{Wp} \log \frac{4p^2 + m_\rho^2}{m_\rho^2} \tag{47}$$

$$\tan \delta_s = -\frac{g_{\text{R}}^2}{16\pi} \frac{p}{W} \frac{1}{W^2 - m_\rho^2} . \tag{48}$$

Equations (47) and (48) are fitted to the phase shift data. In case A, $g_{\text{R}} = 0$ and there is only one fit parameter λ_{R}, in cases B and C we fit the parameters λ_{R}, g_{R} and m_ρ. In order to reduce finite volume polarization and finite lattice spacing effects, we exclude points with $p > 1.5m_\phi$ and small lattice volumes. Only two lowest energy levels from each P sector are used, except in case C where we use 3 lowest levels from the $P = 0$ sector. Both of the momentum sectors are fitted together. We take it as a sign of the consistency of the calculation that the results do not vary significantly if only one of the sectors is included in the fit. The χ^2 values of the fits are 21/19 d.o.f. for case A, 72/32 d.o.f. for B and 63/60 d.o.f. for C. The large χ^2 value for case B is partly due to the very sharp nature of the resonance: $\delta_l(p)$ varies very rapidly in a narrow p-range, and even small unaccounted systematic factors can have a large effect.

The fitted parameters are listed in table 1, and the fitted functions are shown in figures 9 and 10 with solid lines. Case A corresponds to pure lattice ϕ^4 theory, and the fitted value for λ_{R} is 28.1 ± 1.1. This is slightly larger than the perturbative value $\lambda_{\text{R}} = 24 \pm 3$ at the bare lattice coupling $\kappa_\phi = 0.0742$ [24]. However, if we include only the points with $p < 0.6m_\phi$ in the fit, the result is $\lambda_{\text{R}} = 26 \pm 2$.

In cases B and C λ_{R} is 36.8 ± 1.3 and 48.3 ± 2.0, respectively. These are close to but still somewhat larger than the perturbatively calculated pure lattice ϕ^4 theory values 29 ± 3 at $\kappa_\phi = 0.07325$ and 42 ± 7 at $\kappa_\phi = 0.07075$ [24]. In this case one can expect the values to be different, since the coupling to the ρ field affects the renormalization.

The value of the renormalized 3-point coupling g_{R} is 0.598(14) (B) and 1.49(3) (C). The ratio of these values is 0.40(1), which is quite close to the ratio of the bare couplings

$0.008/0.021 \approx 0.38$.

The resonance masses are $m_\rho = 0.5306(13)$ in case B and $0.8206(11)$ in case C. The resonance widths Γ_ρ are calculated from

$$\Gamma_\rho = \frac{g_R^2}{32\pi m_\rho^2} \sqrt{m_\rho^2 - 4m_\phi^2},\tag{49}$$

with the results $\Gamma_\rho = 0.0044(2)$ (B) and $0.0178(7)$ (C). In both cases the resonance is quite narrow: in case B, the ratio Γ_ρ/m_ϕ is only 0.8% and in case C 2.2%.

An alternate method to calculate the resonance mass and width is to use the generic Breit-Wigner relativistic form

$$\tan\delta(p) = \frac{m_\rho \Gamma_\rho}{m_\rho^2 - W^2}.\tag{50}$$

This is valid only in the small neighborhood of the resonance value $\delta \sim \pi/2$. For our data eq. (50) alone does not give a good fit, but if we add the term proportional to λ_R from eq. (47) to the Breit-Wigner phase shift we obtain results comparable to the perturbative ansatz (47–48).

3.8   Wave function representation

The decomposition of the energy eigenstates into states with definite momentum tells us if the number of the states in the correlation function matrices is large enough. The projection to the momentum states can be obtained from the vector $\psi_a = C^{-1/2}(t_0)\Psi_a$, where Ψ_a is an eigenvector of the matrix $D(t)$, eq. (42). After normalizing, the squares of the components $(\psi_a^\alpha)^2$ give the relative contribution of momentum states α to the energy eigenstate a. The eigenvectors should be independent of t, and typically they do not vary significantly until the correlation function fitting range is exceeded.

In figure 11 we show the weights of the physical states which belong to levels 2 and 3 in momentum sectors $P = 0$ and $P = 2\pi/L$. The values have been averaged over the range $1 \leq t \leq 5$. The contribution of ρ is shown with filled circles. In the $P = 0$ sector the 2ϕ cm-momentum p states are as follows: $q^2 = (pL/(2\pi))^2 = 0$ is shown with open circles, $q^2 = 1$ with boxes, and $q^2 = 3$ with triangles. In the $P = 2\pi/L$ sector we enumerate the 2ϕ states with $\mathbf{q}_1$ and define $\mathbf{q}_2 = (0,0,1) - \mathbf{q}_1$. The levels shown are $\mathbf{q}_1 = (0,0,1)$ with open circles, (0,1,1) with boxes, (0,0,2) with triangles and (1,1,1) with crosses. Only levels with non-negligible amplitudes are shown.

The figure shows that away from the level crossing regions the physical states are strongly dominated by only one momentum state. Around the avoided level crossing the physical state is comprised of mostly two momentum states with smoothly varying amplitudes. An exception to this rule occurs in the sector $P = 2\pi/L$ when the level 3

25
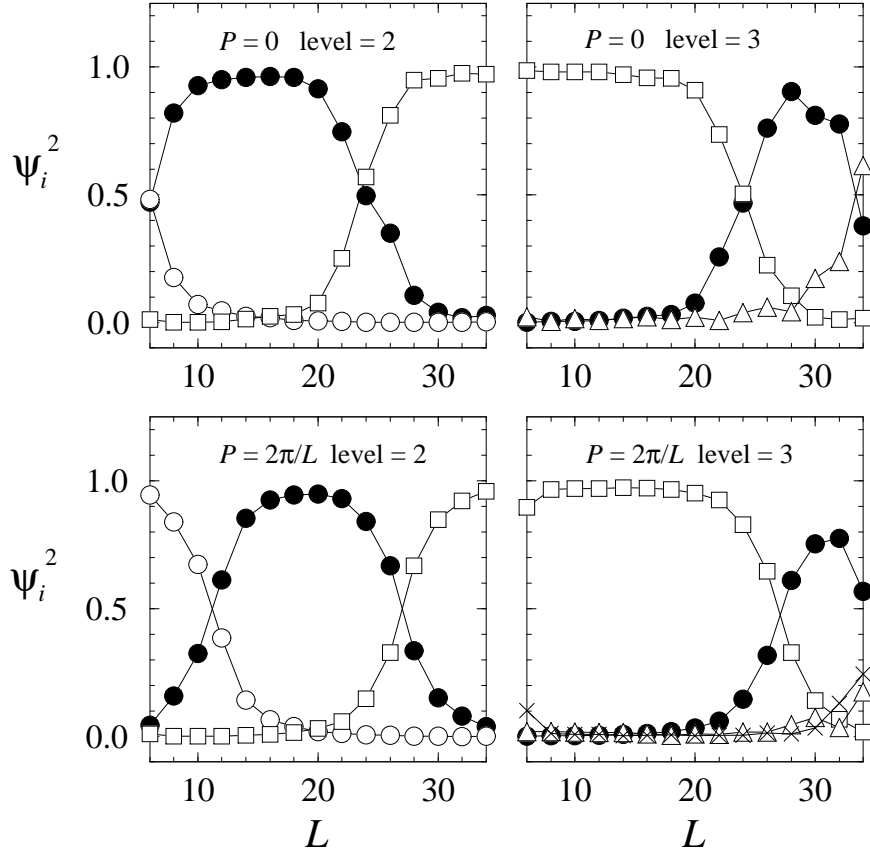
Figure 11: The projections of the eigenstates to the ρ and 2ϕ momentum states in case C. ρ is shown with filled circles, and 2ϕ states with open circles, boxes, triangles and crosses, from the lowest momentum value to the highest. Only states with an appreciable projection are shown.

approaches the avoided crossing with the nearly degenerate levels 4 and 5 ($L \sim 34$). Both of the momentum states $\mathbf{q}_1 = (0, 0, 2)$ and $(1,1,1)$ contribute to the physical state with non-negligible amplitudes.

The strong dominance of only 1 or 2 momentum states in the decompositions of the physical states indicates that the correlation function matrices (38) and (37) have enough states to accurately describe at least 3 lowest energy levels (which are the only ones we used in the numerical analysis). With the parameters used in case C several new states start to approach the resonance mass level after $L \sim 34$. It becomes increasingly difficult to obtain accurate information about the resonance: one needs correlation function matrices with more states and with increased statistical accuracy. In case B this would happen at $L \sim 55$.

4 Derivation of the phase shift formula

In this section we derive the fundamental equation (17). The derivation uses the formalism derived in references [12, 13], generalizing it to encompass non-zero total momentum case. In order to keep the discussion simple, we are working at the level of the relativistic 2-particle quantum mechanics. The generalization to the field theory level can be done, for example, with the Bethe-Salpeter formalism, as discussed by Lüscher [12].

The expansion of the 2-particle scattering wave function in terms of spherical harmonics has a physical meaning only in the center of mass frame. This is especially relevant in the case of resonance scattering, where the resonance channel is an eigenstate of angular momentum. Also, we want to compare the results obtained with both zero-momentum and non-zero momentum scattering sectors, and join the data together in order to construct a more complete picture of the scattering wave functions. To reach this goal it is necessary for us to be able to relate the laboratory frame measurements to the center of mass quantities.

Due to the Bose symmetry the angular momentum $l = $ odd channels have a vanishing scattering amplitude for identical spin-0 particles. Therefore, in the following we shall implicitly assume that the fields carry an extra quantum number making the particles distinguishable, if necessary. The projection to the desired symmetry sector can be made at any stage of the analysis.

4.1 Lorentz transformation of the wave function

Let us consider two spinless bosons of mass m_ϕ in an infinite volume. The state of the system is described by the scalar wave function $\psi(x_1, x_2)$, where $x_i = (x_i^0, \mathbf{x}_i)$ are the 4-dimensional Minkowski space-time coordinates of the particles. The wave function transforms in Lorentz transformations as $\psi \to \psi'$:

$$\psi(x_1, x_2) = \psi'(x_1', x_2') = \psi'(\Lambda x_1, \Lambda x_2), \tag{51}$$

where $(x')^\mu = \Lambda^\mu{}_\nu x^\nu$ denotes the Lorentz transformation of the 4-vector x. The wave function depends on two time coordinates, and the space and time coordinates are mixed in Lorentz transformations. Often it is convenient to consider only the case $x_1{}^0 = x_2{}^0$ (equal time formalism). However, this condition has different physical meanings in different inertial frames and makes the formalism explicitly non-covariant.

The situation can be made simpler by using the special properties of the center of mass frame of the particles. Let us first consider *non-interacting* particles: in any inertial frame, the wave function satisfies the Klein-Gordon equations (we use here the metric tensor sign convention $g_{\mu\nu} = \mathrm{diag}(1, -1, -1, -1)$)

$$(\hat{p}_{i\mu}\hat{p}_i{}^\mu - m_\phi^2)\psi(x_1, x_2) = 0, \quad i = 1, 2 \tag{52}$$

where the standard operator relation $\hat{p}_{i\mu} = -i\partial/\partial x_i{}^\mu$ is understood. Equations (52) can be transformed with the change of variables

$$X = \tfrac{1}{2}(x_1 + x_2) \tag{53}$$
$$x = x_1 - x_2 \tag{54}$$

into the form

$$\left[4(\hat{p}_\mu\hat{p}^\mu - m_\phi^2) + \hat{P}_\mu\hat{P}^\mu\right]\psi(x,X) = 0 \tag{55}$$
$$\hat{p}_\mu\hat{P}^\mu\,\psi(x,X) = 0 \tag{56}$$

where $\hat{p} = (\hat{p}_1 - \hat{p}_2)/2$, and $\hat{P} = \hat{p}_1 + \hat{p}_2$ is the total 4-momentum operator.

In the absence of external potentials, the total momentum is conserved and we can restrict ourselves to eigenfunctions of P even when the 2-particle interaction is turned on:

$$\psi(x,X) = e^{-iP_\mu X^\mu}\phi(x). \tag{57}$$

The center of mass frame is defined as the frame where the space components of the total momentum vanish: $\mathbf{P}^* = 0$ (the index * is used to denote center of mass coordinate and momenta). We shall consider only positive kinetic energy solutions $P_0^* = W_{\text{CM}} > 2m_\phi$. From eq. (56) it follows that $\hat{p}_0^*\phi_{\text{CM}}(x^*) = -i\partial_0\phi(x^*) = 0$. Thus, in the center of mass frame the wave function depends only on the time variable $t^* = X^{*0} = \tfrac{1}{2}(x_1^{*0} + x_2^{*0})$ and the relative separation of the particles $\mathbf{x}^* = \mathbf{x}_1^* - \mathbf{x}_2^*$:

$$\psi_{\text{CM}}(\mathbf{x}^*, t^*) = e^{-iW_{\text{CM}}t^*}\phi_{\text{CM}}(\mathbf{x}^*). \tag{58}$$

Let us now consider the situation in the laboratory frame. The transformation from the laboratory frame to the center of mass frame can be written as $r^{*\mu} = \Lambda^\mu{}_\nu r^\nu$, where r is any position 4-vector and quantities without * refer to the laboratory frame. With the shorthand definition eq. (7), this is

$$r^{*0} = \gamma(r^0 + \mathbf{v}\cdot\mathbf{r}) \tag{59}$$
$$\mathbf{r}^* = \vec{\gamma}(\mathbf{r} + \mathbf{v}r^0) \tag{60}$$

where $\mathbf{v} = \mathbf{P}/P_0$ is the 3-velocity of the center of mass in the laboratory frame. Using the transformation (51), the identity $P_\mu X^\mu = P_\mu^* X^{*\mu}$ and eq. (57), the laboratory frame wave function can be written as $\psi_{\text{L}}(x,X) = \exp(-iP_\mu X^\mu)\phi_{\text{L}}(x)$, where

$$\phi_{\text{L}}(x) = \phi_{\text{L}}(x^0, \mathbf{x}) = \phi_{\text{CM}}(\vec{\gamma}(\mathbf{x} + \mathbf{v}x^0)). \tag{61}$$

Note that ϕ_{L} depends explicitly on $x^0 = x_1{}^0 - x_2{}^0$. However, in the laboratory frame we are interested in the case where both of the particles have equal time coordinate,

28

$x^0 = 0$ (More specifically, on the lattice all 2-particle operators act on single spacelike hyperplane.). In the CM frame this corresponds to the tilted plane $(x^{*0}, \mathbf{x}^*) = (\gamma \mathbf{v} \cdot \mathbf{x}, \vec{\gamma}\, \mathbf{x})$, but because ϕ_{CM} is independent of x^{*0}, the effect of the tilt to the wave function vanishes and eq. (61) has the simple form

$$\phi_{\mathrm{L}}(0, \mathbf{x}) = \phi_{\mathrm{CM}}(\vec{\gamma}\, \mathbf{x}). \tag{62}$$

Equation (62) relates the laboratory frame wave function

$$\psi_{\mathrm{L}}(0, \mathbf{x}, t, \mathbf{X}) = e^{-iW_{\mathrm{L}}t + i\mathbf{P}\cdot\mathbf{X}}\phi_{\mathrm{L}}(0, \mathbf{x}) \tag{63}$$

to the center of mass frame wave function eq. (58). The total energy of the system in the two frames is related by $W_{\mathrm{L}}^2 = W_{\mathrm{CM}}^2 + \mathbf{P}^2$. Finally, from eqs. (55) and (58) we note that ϕ_{CM} satisfies the Helmholtz equation

$$(\nabla_{\mathbf{x}^*}^2 + p^{*2})\phi_{\mathrm{CM}}(\mathbf{x}^*) = 0 \tag{64}$$

where $p^{*2} = (W_{\mathrm{CM}}/2)^2 - m_\phi^2$. Equations (62) and (64) will be of fundamental importance when we consider the wave functions on a torus: the boundary conditions imposed by the torus in the laboratory frame are transformed by eq. (62) into boundary conditions on the solutions eq. (64). In what follows we shall omit the superscript * from the center of mass frame quantities.

4.2   The scattering wave function

The covariant formulation of an interacting two-particle theory is a non-trivial task. However, the details of the interaction are not essential for the problem at hand. For concreteness, we shall describe the interaction with a potential $A_\mu(\mathbf{x})$ in the center of mass frame, without specifying the nature of the potential or how it acts on the wave function. It is sufficient to assume only that the equations that replace the Klein-Gordon equations (52) when A_μ is included admit a square integrable solution and that the potential has a finite range [13]:

$$A_\mu(\mathbf{x}) = 0 \quad \text{for} \quad |\mathbf{x}| > R. \tag{65}$$

Let us assume that there exists R so that eq. (65) is true both in the center of mass and laboratory frames. Then the Klein-Gordon equations (52) hold when $|\mathbf{x}| > R$, and in this region the wave functions eq. (58) and eq. (63) are related by eq. (62).

In the center of mass frame the interaction is spherically symmetric. The wave function can be expanded in spherical harmonics

$$\phi_{\mathrm{CM}}(\mathbf{x}) = \sum_{l=0}^{\infty} \sum_{m=-l}^{l} Y_{lm}(\theta, \varphi)\phi_{lm}(x) \tag{66}$$

29

where $\mathbf{x} = x(\sin\theta\cos\varphi, \sin\theta\sin\varphi, \cos\theta)$. When $x > R$, ϕ_{CM} is a solution of eq. (64), and the functions ϕ_{lm} satisfy the radial differential equation

$$[\frac{\mathrm{d}^2}{\mathrm{d}x^2} + \frac{2}{x}\frac{\mathrm{d}}{\mathrm{d}x} - \frac{l(l+1)}{x^2} + p^2]\phi_{lm}(x) = 0 \tag{67}$$

where $p^2 = (W_{\mathrm{CM}}/2)^2 - m_\phi^2 > 0$. The solutions of eq. (67) can be written as linear combinations of the spherical Bessel functions

$$\phi_{lm}(x) = c_{lm}\left[a_l(p)j_l(px) + b_l(p)n_l(px)\right]. \tag{68}$$

In the region $x < R$ the form of the radial equation for the coefficients ψ_{lm} is unknown. We shall assume that for each l, m there exists an unique regular solution for all values of $W_{\mathrm{CM}} > 2m_\phi$ (for a more detailed discussion, see [12, 13]). The coefficients c_{lm}, a_l and b_l are then determined when the interior and exterior solutions are joined together at $x = R$.

By comparing the function defined in equations (66) and (68) to the definition of the phase shift δ_l given in eq. (2), we can establish the well-known connection between the scattering phase shift and the coefficients a_l and b_l [30]:

$$e^{i2\delta_l(p)} = \frac{a_l(p) + ib_l(p)}{a_l(p) - ib_l(p)}. \tag{69}$$

Since a_l and b_l can be chosen real-valued when $p > 0$, $\delta_l(p)$ is a real analytic function. For a fixed l-sector, the phase shift can now be given in terms of the laboratory frame energy with the relation $p^2 = (W_{\mathrm{L}}^2 - \mathbf{P}^2)/2 - m_\phi^2$.

4.3   Eigenstates on a torus

Let us now study the system in a (laboratory frame) box of size $L \times L \times L$ with periodic boundary conditions. The time direction of the box is taken to be infinite. The laboratory frame wave functions ψ_{L} are periodic with respect to the position of either of the particles:

$$\psi_{\mathrm{L}}(\mathbf{x}_1, \mathbf{x}_2) = \psi_{\mathrm{L}}(\mathbf{x}_1 + \mathbf{n}L, \mathbf{x}_2 + \mathbf{m}L) \qquad \text{for all} \quad \mathbf{n}, \mathbf{m} \in \mathbf{Z}^3. \tag{70}$$

The form of the wave function ψ_{L} is given by eq. (63)

$$\psi_{\mathrm{L}}(\mathbf{x}_1, \mathbf{x}_2) = e^{i\mathbf{P}\cdot(\mathbf{x}_1 + \mathbf{x}_2)/2}\phi_{\mathrm{L}}(\mathbf{x}_1 - \mathbf{x}_2). \tag{71}$$

Equations (70) and (71) together yield the result

$$\begin{aligned} \mathbf{P} &= (2\pi/L)\,\mathbf{d} \\ \phi_{\mathrm{L}}(\mathbf{x}) &= (-1)^{\mathbf{d}\cdot\mathbf{n}}\phi_{\mathrm{L}}(\mathbf{x} + \mathbf{n}L) \end{aligned} \qquad \mathbf{d}, \mathbf{n} \in \mathbf{Z}^3. \tag{72}$$

30

The total momentum $\mathbf{P}$ is conserved, and the quantization rule (72) divides the wave functions into discrete total momentum sectors, which we classify by the vector $\mathbf{d} \in \mathbf{Z}^3$. We are mostly interested in sectors $\mathbf{d} = (0,0,0)$ and $\mathbf{d} = (0,0,1)$ (and permutations). Depending on the value of $\mathbf{d}$, the function ϕ_L is either periodic or antiperiodic with period length L.

Now we can use equation (62) to obtain the corresponding periodicity rule for the center of mass wave function. For a fixed vector $\mathbf{d}$,

$$\phi_{CM}(\mathbf{x}) = (-1)^{\mathbf{d} \cdot \mathbf{n}} \phi_{CM}(\mathbf{x} + \vec{\gamma}\,\mathbf{n}L) \qquad \text{for all} \quad \mathbf{n} \in \mathbf{Z}^3. \tag{73}$$

The energy W_L and the box size L determine $\vec{\gamma}$, since $\mathbf{v} = \mathbf{P}/W_L = 2\pi \mathbf{d}/(LW_L)$. Equation (73) has an simple interpretation: the center of mass system sees the laboratory frame torus *expanded* by the fraction γ to the direction of the total momentum, while the length scales to the perpendicular directions are preserved. For compactness, we shall call the functions obeying the rule (73) $\mathbf{d}$-*periodic* functions.

Let us note that the Lorentz-contraction reduces the cubic symmetry of the original box: if $\mathbf{d} = (0,0,1)$, the volume changes to $L \times L \times (\gamma L)$, which has tetragonal point symmetry. If $\mathbf{d} = (1,1,0)$, the square in the $(1,2)$-plane is deformed into a skewed parallelogram with diagonals $\sqrt{2}L$ and $\gamma\sqrt{2}L$; only orthorhombic point symmetry remains. In general, if all 3 components of $\mathbf{d}$ are non-zero, the volume becomes a parallelepiped with all angles between the faces non-orthogonal. This reduction of the symmetry is further discussed in section 5.

In the center of mass frame, the interaction has the same period as the wave function but without the antiperiodicity:

$$A_{L,\mu}(\mathbf{x}) = \sum_{\mathbf{n} \in \mathbf{Z}^3} A_\mu(\mathbf{x} + \vec{\gamma}\,\mathbf{n}L)\,. \tag{74}$$

Assuming that $L > 2R$, we can define the "exterior" region

$$\Omega_{CM} = \{\mathbf{r} \in \mathbf{R}^3 \big| |\mathbf{r} - \vec{\gamma}\,\mathbf{n}L| > R \text{ for all } \mathbf{n} \in \mathbf{R}^3\} \tag{75}$$

where the potential A_L vanishes. In this region ϕ_{CM} satisfies the Helmholtz equation (64)

$$(\nabla^2 + p^2)\phi_{CM}(\mathbf{x}) = 0\,. \tag{76}$$

In the region $R < r < L/2$ the solution ϕ_{CM} of the Helmholtz equation can be expanded in spherical harmonics and spherical Bessel functions (see eqs. (66) and (68)). Following section 4.2, it can be shown that there exists a unique solution of the full interacting equations of motion in $\mathbf{R}^3$ which coincides with ϕ_{CM} in the region Ω_{CM}.

Our task is now to fit together the boundary condition eq. (73) and the spherical components given by eq. (66). We perform this by finding the general form of the Helmholtz equation and expand it in spherical harmonics and Bessel functions in the region $R < r < L/2$.

4.4 Singular d-periodic solutions of the Helmholtz equation

In this section we derive the general form of the solutions of the Helmholtz equation obeying the periodicity rule eq. (73). With the exception of the **d**-periodicity, our calculation follows the one by Lüscher (sections 3 and 4 in ref. [13]), and in our discussion we shall omit technical details which can be directly recovered by appropriate generalizations of Lüscher's formalism.

In the following we shall call a function ϕ a singular **d**-periodic solution of the Helmholtz equation, when it is a smooth function defined for all $\mathbf{x} \neq \vec{\gamma}\,\mathbf{n}L$, $\mathbf{n} \in \mathbf{Z}^3$, and it satisfies the Helmholtz equation (76)

$$(\nabla^2 + p^2)\phi(\mathbf{x}) = 0 \tag{77}$$

for some value of $p > 0$, and obeys the **d**-periodicity rule

$$\phi(\mathbf{x}) = (-1)^{\mathbf{d}\cdot\mathbf{n}}\phi(\mathbf{x} + \vec{\gamma}\,\mathbf{n}L) \qquad \text{for all } \mathbf{n} \in \mathbf{Z}^3\,. \tag{78}$$

Furthermore, we require that the function is bounded by a power of $1/|\mathbf{x}|$ near the origin:

$$\lim_{\mathbf{x}\to 0} |\mathbf{x}^{\Lambda+1}\phi(\mathbf{x})| < \infty \tag{79}$$

for some positive integer Λ, which we call the degree of ϕ.

In what follows we shall also assume that the value of p is not "singular":

$$p \neq \frac{2\pi}{L}|\vec{\gamma}^{\,-1}(\mathbf{n} + \tfrac{1}{2}\mathbf{d})| \qquad \text{for all } \mathbf{n} \in \mathbf{Z}^3. \tag{80}$$

For singular values of p the Helmholtz equation admits plane wave solutions which complicate the situation. These values require a separate treatment, which we shall omit here; the treatment is a straightforward generalization of the non-singular case [13].

We can now define the Green function

$$G^{\mathbf{d}}(\mathbf{x}; p) = \gamma^{-1}L^{-3}\sum_{\mathbf{k}\in\Gamma} \frac{e^{i\mathbf{k}\cdot\mathbf{x}}}{\mathbf{k}^2 - p^2} \tag{81}$$

where the sum is over the momentum lattice

$$\Gamma = \left\{\mathbf{k} \in \mathbf{R}^3 \,\middle|\, \mathbf{k} = \frac{2\pi}{L}\vec{\gamma}^{\,-1}(\mathbf{n} + \tfrac{1}{2}\mathbf{d}) \text{ for some } \mathbf{n} \in \mathbf{Z}^3\right\}. \tag{82}$$

Since p is non-singular, function (81) is well-defined. If now $\mathbf{k} = (2\pi/L)\vec{\gamma}^{\,-1}(\mathbf{m} + \tfrac{1}{2}\mathbf{d})$ for some $\mathbf{m} \in \mathbf{Z}^3$, then

$$\mathbf{k}\cdot(\mathbf{x} + \vec{\gamma}\,\mathbf{n}L) = \mathbf{k}\cdot\mathbf{x} + \pi\mathbf{d}\cdot\mathbf{n} + 2\pi\mathbf{m}\cdot\mathbf{n} \qquad \text{for all } \mathbf{n} \in \mathbf{Z}^3\,, \tag{83}$$

and the function $G^{\mathbf{d}}(\mathbf{x}; p)$ is obviously **d**-periodic. It satisfies the equation

$$(\nabla^2 + p^2)G^{\mathbf{d}}(\mathbf{x}; p) = - \sum_{\mathbf{n} \in \mathbf{Z}^3} (-1)^{\mathbf{d} \cdot \mathbf{n}} \delta(\mathbf{x} + \vec{\gamma}\, \mathbf{n}\mathbf{L}) \,. \tag{84}$$

The behavior of $G^{\mathbf{d}}$ around the origin $\mathbf{x} = 0$ is given by

$$G^{\mathbf{d}}(\mathbf{x}; p) = \frac{p}{4\pi} n_0(px) + (\text{regular part at } \mathbf{x} = 0) \tag{85}$$

which follows from the fact that the Bessel function n_0 satisfies the equation

$$(\nabla^2 + p^2)\, n_0(p|\mathbf{x}|) = -\frac{4\pi}{p}\delta(\mathbf{x}) \,. \tag{86}$$

Thus, $G^{\mathbf{d}}$ is an example of singular **d**-periodic solutions of the Helmholtz equation.

Further solutions can be obtained by differentiating $G^{\mathbf{d}}$ with respect to $\mathbf{x}$. Let us define functions

$$G^{\mathbf{d}}_{lm}(\mathbf{x}; p) = \mathcal{Y}_{lm}(\nabla)G^{\mathbf{d}}(\mathbf{x}; p) \tag{87}$$

where we have introduced the harmonic polynomials $\mathcal{Y}_{lm}(\mathbf{x}) = x^l Y_{lm}(\theta, \varphi)$. Since $\mathcal{Y}_{lm}(\nabla)$ commutes with ∇^2, the functions $G^{\mathbf{d}}_{lm}$ are singular **d**-periodic solutions of the Helmholtz equation. Also, it can be shown that the functions $G^{\mathbf{d}}_{lm}$ form a complete set of solutions in the sense that any singular **d**-periodic solution of degree Λ is a linear combination of the functions $G^{\mathbf{d}}_{lm}(\mathbf{x}; p)$ with $l \leq \Lambda$ [13].

As discussed in section 4.2, when $0 < x < L/2$ the functions $G^{\mathbf{d}}_{lm}$ can be expanded in spherical harmonics. The expansion has the form

$$G^{\mathbf{d}}_{lm}(\mathbf{x}; p) = \frac{(-1)^l p^{l+1}}{4\pi} \left\{ n_l(px)Y_{lm}(\theta, \varphi) + \sum_{l'=0}^{\infty} \sum_{m'=-l}^{l} M^{\mathbf{d}}_{lm,l'm'}(p)\, j_{l'}(px)Y_{l'm'}(\theta, \varphi) \right\} \tag{88}$$

where the part singular at $\mathbf{x} = 0$ is directly computable from the action of $\mathcal{Y}_{lm}(\nabla)$ to the function $n_0(px)$. The regular part contains coefficients $M^{\mathbf{d}}_{lm,l'm'}(p)$; in practice, we need only the first few of the coefficients, but for completeness, we give the general expression:

$$M^{\mathbf{d}}_{lm,l'm'}(p) = \gamma^{-1}\frac{(-1)^l}{\pi^{3/2}} \sum_{j=|l-l'|}^{l+l'} \sum_{s=-j}^{j} \frac{i^j}{q^{j+1}} Z^{\mathbf{d}}_{js}(1; q^2)C_{lm,js,l'm'} \,, \tag{89}$$

where we have defined

$$q = \frac{pL}{2\pi} \,. \tag{90}$$

The tensor $C_{lm,js,l'm'}$ can be written in terms of Wigner $3j$-symbols

$$C_{lm,js,l'm'} = (-1)^{m'} i^{l-j+l'} \sqrt{(2l+1)(2j+1)(2l'+1)} \begin{pmatrix} l & j & l' \\ m & s & -m' \end{pmatrix} \begin{pmatrix} l & j & l' \\ 0 & 0 & 0 \end{pmatrix} \,. \tag{91}$$

The generalized zeta function in eq. (89) is defined through the equation

$$Z_{lm}^{\mathbf{d}}(s; q^2) = \sum_{\mathbf{r} \in P_{\mathbf{d}}} \mathcal{Y}_{lm}(\mathbf{r})(\mathbf{r}^2 - q^2)^s \,, \tag{92}$$

where the summation is over the set

$$P_{\mathbf{d}} = \{\mathbf{r} \in \mathbf{R}^3 \,|\, \mathbf{r} = \vec{\gamma}^{\,-1}(\mathbf{n} + \tfrac{1}{2}\mathbf{d}) \ \text{ for some } \mathbf{n} \in \mathbf{Z}^3\} \,. \tag{93}$$

The sum in eq. (92) converges when $\mathrm{Re}\, 2s > l + 3$, and can be analytically continued to the whole complex plane. The method for evaluating the zeta function at $s = 1$ is discussed in section 5.2.

If we now choose the sector $\mathbf{d} = 0$, the laboratory frame and the center of mass frame coincide, $\gamma \to 1$ and $P_{\mathbf{d}} \to \mathbf{Z}^3$, and equations (88–92) reduce to the form given in ref. [13]. Since the derivation of the above formulae is lengthy and analogous to the discussion therein, we shall omit it here.

5 Symmetry considerations

When the laboratory frame and the center of mass frame coincide, the system exhibits a cubic symmetry and the wave functions transform according to the representations of the cubic group $O(3, \mathbf{Z})$. This symmetry was utilized by Lüscher [13] to considerably simplify the expressions for the energy spectrum. However, as mentioned in section 4.3, if the two frames are not equivalent, the Lorentz boost from the laboratory frame to the center of mass frame in effect "deforms" the cubical volume and only some subgroup of the original cubic point symmetry group remains.

The deformations caused by the Lorentz boost are of a special kind: the length scales to the direction of the boost are multiplied by γ, whereas the perpendicular length scales are preserved. Depending on the orientation of the boost with respect to the directions defined by the periodicity of the (laboratory frame) torus, we are left with different subgroups of the cubic symmetry. First, let us consider a boost along one of the coordinate axes, say $\mathbf{d} = (0, 0, d)$. The geometry of the box changes $(1, 1, 1) \to (1, 1, \gamma)$, and the relevant symmetry group is the tetragonal point group D_{4h}. This group has 16 elements: 4 rotations through an angle $(n\pi/2)$, where $n = 0, 1, 2, 3$, around the x_3-axis; 4 rotations of an angle π around directions $\mathbf{e}_1$, $\mathbf{e}_2$, $\mathbf{e}_1 + \mathbf{e}_2$ and $\mathbf{e}_1 - \mathbf{e}_2$; and all eight of the above multiplied by the reflection with respect to the (1,2)-plane.

When $\mathbf{d} \propto (1, 1, 0)$, the unit square in the (1,2)-face is deformed into a parallelogram with edges of length $[(1 + \gamma^2)/2]^{1/2}$ and with an angle $2 \tan^{-1} \gamma$ between adjacent edges. The symmetry group is the orthorhombic group D_{2h} with 8 elements.

The relevant point groups and the boost vectors are classified in table 2. All of the groups contain the parity transformation $\mathbf{x} \to -\mathbf{x}$. The group C_i has only two elements,

34

$\mathbf{d}$	point group	classification	N_{elements}
$(0,0,0)$	O_h	cubic	48
$(0,0,a)$	D_{4h}	tetragonal	16
$(0,a,a)$	D_{2h}	orthorhombic	8
$(0,a,b)$	C_{2h}	monoclinic	4
(a,a,a)	D_{3d}	trigonal	12
(a,a,b)	C_{2h}	monoclinic	4
(a,b,c)	C_i	triclinic	2

Table 2: The classification of the Lorentz boosts on a torus and the reduction of the cubic symmetry. The first column displays the direction of the boost (modulo permutations); the numbers a, b and c are all taken to be different from each other and from 0. The notation used for the groups is the Schonflies notation. [31]

the identity element and the parity transformation; it results from a boost where the length of all of the 3 components of $\mathbf{d}$ are different from each other.

In the simulations described in this paper we use only the two lowest total momentum sectors, $|\mathbf{d}| = 0$ or 1. The next two total momentum sectors suffer from the fact that already the two lowest energy levels are nearly degenerate (see section 2.1), which limits the usability of these sectors in practical Monte Carlo simulations. Thus, in the following we discuss mainly only the cubic and tetragonal symmetry groups O_h and D_{4h}. We shall explicitly select vectors $\mathbf{d} = \mathbf{0}$ (cubic symmetry, O_h) and $\mathbf{d} = (0,0,1)$ (tetragonal symmetry, D_{4h}). This choice gives the x_3-axis a special status, and many calculations are simpler to perform; naturally, the final results are independent of the choice of the axis. At this stage we need not invoke the antiperiodicity of the wave functions to the x_3-direction, and the formulae given below are valid for any $\mathbf{d} = (0,0,n)$.

The symmetry properties of the zeta function $Z_{lm}^{\mathbf{d}}$ follow directly from the definition eq. (92) and the properties of the spherical harmonic functions under symmetry operations. In particular, let us consider the following transformations: parity transformation $\mathbf{x} \to -\mathbf{x}$, a reflection $\mathbf{x} \to (x_1, -x_2, x_3)$, and a rotation of an angle $\pi/2$ around x_3-axis. These operations yield

$$
\begin{aligned}
Z_{lm}^{\mathbf{d}}(s;q^2) &= 0 \quad \text{if } l \text{ is odd} \\
Z_{lm}^{\mathbf{d}}(s;q^2) &= Z_{l-m}^{\mathbf{d}}(s;q^2) \\
Z_{lm}^{\mathbf{d}}(s;q^2) &= 0 \quad \text{if } m \neq 4n,\, n \in \mathbf{Z}
\end{aligned}
\tag{94}
$$

The first property is valid for all of the groups listed in table 2. The cubic group has additional symmetries absent from the octahedral group. Most important of these are

$Z_{20}^0 = 0$ and $Z_{44}^0 = \sqrt{70}/14\, Z_{40}^0$. These differences have an effect in the energy spectrum calculation.

Using the above properties of the zeta function and symmetries of the $3j$-symbols [31, 32] we can derive symmetry relations for the matrix elements $M^{\mathbf{d}}_{lm,l'm'}$ defined in eq. (89):

$$
\begin{aligned}
M^{\mathbf{d}}_{lm,l'm'} &= 0 && \text{if } l' \neq l \pmod 2 \\
M^{\mathbf{d}}_{lm,l'm'} &= 0 && \text{if } m' \neq m \pmod 4 \\
M^{\mathbf{d}}_{lm,l'm'} &= M^{\mathbf{d}}_{l'm',lm} = M^{\mathbf{d}}_{l(-m),l'(-m')}\,.
\end{aligned}
\tag{95}
$$

In table 3 we list the expressions of $M^{\mathbf{d}}_{lm,l'm'}$ for $l, l' \leq 3$. In order to simplify the table, we have defined

$$
w_{lm} = \frac{1}{\pi^{3/2}\sqrt{2l+1}}\gamma^{-1}q^{-l-1} Z^{\mathbf{d}}_{lm}(1; q^2)\,.
\tag{96}
$$

The necessary $3j$-symbol values can be found in the literature [32]. Matrix elements missing from the table are either zero, or can be obtained with the symmetry relations (95).

The table 3 can be compared to table E.1 in ref. [13], which lists the matrix elements for $\mathbf{d} = 0$. The main difference is the appearance of functions w_{20}, w_{44} and w_{64} in table 3. If we set $\mathbf{d} = 0$, then $w_{20} \to 0$, $w_{44} \to \sqrt{70}/14\, w_{40}$ and $w_{64} \to -\sqrt{14}/2\, w_{60}$, and Lüscher's result is recovered.

If we further reduce the symmetry of the system, more of the elements become non-zero. For example, in the case of the group D_{2h} the element $w_{22} \neq 0$; and finally, for a generic boost vector $\mathbf{d}$ the relevant group is C_i and all $w_{(2l)m} \neq 0$.

5.1 Energy spectrum

We are now in a position to consider the singular $\mathbf{d}$-periodic solutions of the equations of motion that contain the 2-particle interaction. The general form of the solutions of the equations of motion in the region $R < |\mathbf{x}| < L/2$ was given in equations (66) and (68). On the other hand, in section 4.4 it was noted that the functions $G^{\mathbf{d}}_{lm}(\mathbf{x}, p^2)$ form a complete set of singular $\mathbf{d}$-periodic solutions when $l \leq \Lambda$, where Λ is the degree of the function. When we demand that the functions are equal, we have

$$
\sum_{l=0}^{\Lambda}\sum_{m=-l}^{l} v_{lm} G^{\mathbf{d}}_{lm}(\mathbf{x}, p^2) = \sum_{l=0}^{\Lambda}\sum_{m=-l}^{l} c_{lm}[a_l(p)j_l(px) + b_l(p)n_l(px)]\, Y_{lm}(\theta, \varphi)
\tag{97}
$$

for some constants c_{lm} and v_{lm}. Using equation (88), we can eliminate v_{lm} and obtain

$$
c_{lm}a_l(p) = \sum_{l'=0}^{\Lambda}\sum_{m'=-l'}^{l'} c_{l'm'}b_{l'}(p) M^{\mathbf{d}}_{l'm',lm}(p)\,.
\tag{98}
$$

36

l	m	l'	m'	$M^{\mathbf{d}}_{lm,l'm'}$					
0	0	0	0	w_{00}					
1	0	1	0	w_{00}	$+2w_{20}$				
1	1	1	1	w_{00}	$-w_{20}$				
2	0	0	0		$-\sqrt{5}\,w_{20}$				
2	0	2	0	w_{00}	$+\frac{10}{7}w_{20}$	$+\frac{18}{7}w_{40}$			
2	1	2	1	w_{00}	$+\frac{5}{7}w_{20}$	$-\frac{12}{7}w_{40}$			
2	2	2	-2				$\frac{3}{7}\sqrt{70}\,w_{44}$		
2	2	2	2	w_{00}	$-\frac{10}{7}w_{20}$	$+\frac{3}{7}w_{40}$			
3	0	1	0		$-\frac{3}{7}\sqrt{21}\,w_{20}$	$-\frac{4}{7}\sqrt{21}\,w_{40}$			
3	1	1	1		$-\frac{3}{7}\sqrt{14}\,w_{20}$	$+\frac{3}{7}\sqrt{14}\,w_{40}$			
3	3	1	-1				$2\sqrt{3}\,w_{44}$		
3	0	3	0	w_{00}	$+\frac{4}{3}w_{20}$	$+\frac{18}{11}w_{40}$		$+\frac{100}{33}w_{60}$	
3	1	3	1	w_{00}	$+w_{20}$	$+\frac{3}{11}w_{40}$		$-\frac{25}{11}w_{60}$	
3	2	3	-2				$\frac{3}{11}\sqrt{70}\,w_{44}$		$+\frac{10}{11}\sqrt{14}\,w_{64}$
3	2	3	2	w_{00}		$-\frac{21}{11}w_{40}$		$+\frac{10}{11}w_{60}$	
3	3	3	-1				$\frac{3}{11}\sqrt{42}\,w_{44}$		$-\frac{5}{33}\sqrt{210}\,w_{64}$
3	3	3	3	w_{00}	$-\frac{5}{3}w_{20}$	$+\frac{9}{11}w_{40}$		$-\frac{5}{33}w_{60}$	

Table 3: Matrix elements $M^{\mathbf{d}}_{lm,l'm'}$ for $\mathbf{d} = (0,0,d)$ and for $l, l' \leq 3$.

A non-zero solution for the vector c_{lm} exists if the determinant of a matrix we are about to construct vanishes. We rewrite eq. (98) as a matrix equation $C(A - BM) = 0$, where matrix $A_{(lm),(l'm')} = a_l(p)\delta_{l,l'}\delta_{m,m'}$ (likewise for B). Since A and B are diagonal and all the diagonal elements of $A - iB$ are non-zero, we can utilize relation (69) to define the phase shift matrix

$$e^{2i\delta} = (A + iB)/(A - iB) \tag{99}$$

Noting that $A - BM = (i/2)(A + iB)(M - i) - (A - iB)(M + i)$, we can factor out $(A - iB)$ and the determinant condition acquires the compact form

$$\det\left[e^{2i\delta}(M - i) - (M + i)\right] = 0. \tag{100}$$

This equation is equivalent to eq. (4.10) in ref. [13].

Using the symmetry properties (95) of the matrix elements $M^{\mathbf{d}}_{lm,l'm'}$, it is evident that the sectors with even and odd l in eq. (98) are completely independent of each other. This is a direct consequence of the symmetry of the system under reflections $\mathbf{x} \to -\mathbf{x}$: reflection symmetry implies that the energy eigenstates are also eigenstates of parity, and the the spherical harmonics have parity $P = (-1)^l$.

Generally, the energy eigenstates will belong to some irreducible representation of the symmetry group of the system. The cubic group of proper rotations O has 5 representations: 2 dimension 1 representations A_1 and A_2, 2-dimensional representation E, and 3-dimensional representations T_1 and T_2. O_h includes the parity transformation and the number of representations is doubled to parity even and odd representations, which are denoted with A_1^+ and A_1^- (likewise for the other representations). The tetragonal group D_4 has 4 1-dimensional representations A_1, A_2, B_1, B_2, and one 2-dimensional representation E [31]. Again, the group D_{4h} doubles these to parity even ($^+$) and odd ($^-$) representations.

The cubic symmetry has been covered in detail in [13], and we concentrate here on the tetragonal symmetry. The representations $\Gamma^{(j)}$ of $O(3)$ with $l \leq 3$ are reduced into irreducible representations of D_{4h} as follows:

$$
\begin{aligned}
\Gamma^{(0)} &= A_1^+ \\
\Gamma^{(1)} &= A_2^- \oplus E^- \\
\Gamma^{(2)} &= A_1^+ \oplus B_1^+ \oplus B_2^+ \oplus E^+ \\
\Gamma^{(3)} &= A_2^- \oplus B_1^- \oplus B_2^- \oplus 2\,E^-
\end{aligned}
\tag{101}
$$

The representations can be identified by using character tables [31] or by enumerating harmonic polynomials of degree l which transform according to the representations of D_{4h}. The basis polynomials for each of the representations are listed in table 4 for $l \leq 3$; the polynomials are linear combinations of the harmonic polynomials $\mathcal{Y}_{lm}(\mathbf{x})$ for each

representation	$l=0$	$l=1$	$l=2$	$l=3$	indices
A_1^+	1		$x_3^2-\frac{1}{3}x^2$		
A_2^-		x_3		$x_3^3-\frac{3}{5}x^2 x_3$	
B_1^+			$x_1^2-x_2^2$		
B_2^+			$x_1 x_2$		
B_1^-				$x_1 x_2 x_3$	
B_2^-				$(x_1^2-x_2^2)x_3$	
E^+			$x_i x_3$		$i=1,2$
E^-		x_i		$(x_i^2-\frac{3}{5}x^2)x_i$	$i=1,2$
				$(x_i^2-x_3^2)x_j$	$(i,j)=(1,2),(2,1)$

Table 4: The basis polynomials of the irreducible representations of D_{4h}.

l-sector. The representation E^- occurs twice in the reduction of $\Gamma^{(3)}$ and has two sets of basis polynomials.

The fact that the eigenstates belong to the irreducible representations of the tetragonal group becomes evident when we study closer the matrix elements $M^{\mathbf{d}}_{lm,l'm'}$: let the angular momentum cutoff $\Lambda=3$, and let us look at the even l-sector of the matrix M (the odd l-values are decoupled in any case). From table 3 we observe that M has a block diagonal form $(m_{lm,l'm'}=M^{\mathbf{d}}_{lm,l'm'})$

$$M=\begin{pmatrix} m_{00,00} & m_{00,20} & & & & \\ m_{20,00} & m_{20,20} & & & & \\ & & m_{2-1,2-1} & & & \\ & & & m_{21,21} & & \\ & & & & m_{2-2,2-2} & m_{2-2,22} \\ & & & & m_{22,2-2} & m_{22,22} \end{pmatrix} \qquad (102)$$

The upper left 2×2 matrix transforms according to the representation A_1^+, the two equal elements at the center comprise the two components of the 2-dimensional representation E^+, and if we diagonalize the lower right 2×2 matrix and symmetrize with equations (95), we obtain diagonal elements $\frac{1}{2}(m_{22,22}+m_{2-2,2-2})\pm\frac{1}{2}(m_{22,2-2}+m_{2-2,22})$ which operate on B_1^+ and B_2^+, respectively.

The sector l odd decomposes in an analogous way. In the following we study the sectors

39

A_1^+ and A_2^-, E^-, which are relevant for the scalar and vector scattering channels in infinite volume.

5.1.1 A_1^+ -sector

First, let us consider the case where the angular momentum cutoff $\Lambda = 0$ or 1. From the reduction eq. (101) and table 4 we see that only $M_{00,00}^{\mathbf{d}}$ belongs to this sector, and eq. (100) is one-dimensional. It can be written to the form

$$\tan \delta_0(p) = \frac{1}{M_{00,00}^{\mathbf{d}}} = \frac{\gamma q \pi^{3/2}}{Z_{00}^{\mathbf{d}}(1; q^2)} \qquad q = \frac{L}{2\pi}p \tag{103}$$

where eq. (96) was used in the second equality. This is the fundamental result given in eqs. (17–18), and used in the simulations described in section 3.

If $\Lambda = 2$ or 3, then the sector $l = 2$ is included, and the matrix in eq. (100) is 2-dimensional. The determinant condition then mixes together phase shifts δ_0 and δ_2, corresponding to the infinite volume $l = 0$ scalar and $l = 2$ tensor scattering channels:

$$[e^{2i\delta_0}(m_{00} - i) - (m_{00} + i)][e^{2i\delta_2}(m_{22} - i) - (m_{22} + i)]$$
$$= m_{20}^2(e^{2i\delta_0} - 1)(e^{2i\delta_2} - 1), \tag{104}$$

where we defined $m_{ab} \equiv M_{a0,b0}^{\mathbf{d}}$. If $\delta_2 = 0$ (mod π), eq. (104) reduces immediately to equation (103), as expected. Let us now consider the case $\delta_2 \neq 0$. Usually it is reasonable to assume that the low energy scattering amplitude is dominated by the lowest l-channel and that the phase shifts at higher l:s are small. If we expand $\delta_0 = \delta_0^0 + \Delta_0$, where δ_0^0 satisfies eq. (103), the first order correction due to eq. (104) is

$$\Delta_0(p) = -\frac{m_{20}^2}{m_{00}^2 + 1}\delta_2(p). \tag{105}$$

The function $m_{20}^2/(m_{00}^2 + 1)$ is not naturally small: for example, for the data in case C in section 3 it varies in the range $0.1 - 14$. When $p \to 0$, it diverges as p^{-4} (for fixed γ and L). However, this is not a problem, since it is offset by $\delta_2(p) \sim p^5$ behavior at small p. Nevertheless, there is no "built-in" mechanism which would automatically render the coupling between the $l = 2$ channel and the $l = 0$ channel small. In order for the eq. (103) to be a good approximation, the phase shift $\delta_2(p)$ has to be small due to the physics of the interacting particles. Luckily, the case is usually so: the scattering of two particles is dominated by the lowest allowed angular momentum channel. For the model used in section 3, the good fit of the data to the perturbative ansatz supports this view.

It should be noted that if $\delta_2(p)$ is not small, it becomes impossible to extract the phase shift functions from the energy spectrum: there are two unknown functions $\delta_0(p)$ and

40

$\delta_2(p)$ but only one equation (104). Naturally, if the phase shifts are known, it is still possible to calculate the energy spectrum.

In the $\mathbf{d} = 0$ sector the matrix element $M^{\mathbf{d}}_{20,00}$ vanishes and equation (104) reduces to equation (103) and to a similar equation for $\delta_2(p)$. The lowest angular momentum channel mixing with the scalar $l = 0$ channel is $l = 4$. In this case one can derive expressions similar to eqs. (104) and (105), with the substitution $l = 2 \to 4$ [13].

5.1.2 A_2^- and E^- -sectors

A_2^- and E^- -sectors are important for scattering through the $l = 1$ vector channel in the infinite volume; the most famous example being the $\pi\pi \leftrightarrow \rho$ -scattering in QCD. Let us assume that the angular momentum cutoff $\Lambda \leq 3$. If the cubic symmetry were unbroken, $O(3)$ representation $\Gamma^{(1)}$ would correspond to single 3 dimensional cubic representation T^-. The situation is now complicated by the appearance of two tetragonal representations already at the lowest angular momentum level. The breaking of the cubic symmetry implies that each eigenstate splits into two states with non-degenerate energies.

When the energy spectrum of the system is measured, one has to know to which of the two representations the state corresponding to the energy level belongs. The phase shift $\delta_1(p)$ is obtained from the determinant condition (100)

$$\tan \delta_1(p) = \frac{1}{M^{\mathbf{d}}(\Gamma_{D_{4h}})} \tag{106}$$

where, using table 3,

$$M^{\mathbf{d}}(A_2^-) = \frac{q^{-1}}{\gamma\pi^{3/2}} \Big[Z^{\mathbf{d}}_{00}(1;q^2) + \frac{2}{\sqrt{5}} q^{-2} Z^{\mathbf{d}}_{20}(1;q^2) \Big] \tag{107}$$

$$M^{\mathbf{d}}(E^-) = \frac{q^{-1}}{\gamma\pi^{3/2}} \Big[Z^{\mathbf{d}}_{00}(1;q^2) - \frac{1}{\sqrt{5}} q^{-2} Z^{\mathbf{d}}_{20}(1;q^2) \Big] . \tag{108}$$

It is possible to construct operators which transform according to the representations A_2^- and E^-. Operators $O(A_2^-)$ decouple from eigenstates which belong to the representation E^- (and vice versa). The correlation function matrix constructed from operators $O(A_2^-)$ gives energy eigenvalues which can be used to calculate the phase shift through eq. (107); similarly eq. (108) is used for the eigenvalues from $O(E^-)$ correlation matrix.

If we set $d \to 0$, then $Z^{\mathbf{d}}_{20} \to 0$, $\gamma \to 1$, and equations (107) and (108) become degenerate. Equation (106) reduces to form similar to the $\delta_0(p)$ equation (103) [13].

5.2 Evaluation of the zeta function

The method for evaluating the zeta function when $\mathbf{d} = 0$ has been described in detail by M. Lüscher [13]. The formalism used there is easily adaptable to the $\mathbf{d} \neq 0$ -case, and here

41

we shall give the necessary formulae for numerically evaluating the zeta function without derivation.

Let us define a *heat kernel* of the Laplace operator on a **d**-periodic torus of size $(2\pi)^3$ (so that the periodicity is given by $\phi(\mathbf{x}) = (-1)^{\mathbf{d} \cdot \mathbf{n}} \phi(\mathbf{x} + 2\pi \vec{\gamma} \mathbf{n})$, cf. equation (73))

$$K_{lm}^{\mathbf{d}}(t, \mathbf{x}) = (2\pi)^{-3/2} \sum_{\mathbf{r} \in P_d} \mathcal{Y}_{lm}(\mathbf{r}) \exp(i\mathbf{r} \cdot \mathbf{x} - t\mathbf{r}^2) \tag{109}$$

$$= \gamma(4\pi t)^{-3/2} \frac{i^l}{(2t)^l} \sum_{\mathbf{n} \in \mathbf{Z}^3} (-1)^{\mathbf{d} \cdot \mathbf{n}} \mathcal{Y}_{lm}(\mathbf{x} + 2\pi \vec{\gamma} \mathbf{n}) \exp[-\frac{1}{4t}(\mathbf{x} + 2\pi \vec{\gamma} \mathbf{n})^2] \tag{110}$$

where $P_{\mathbf{d}} = \{\mathbf{r} \in \mathbf{Z}^3 \,|\, \mathbf{r} = \vec{\gamma}^{-1}(\mathbf{n} + \frac{1}{2}\mathbf{d}), \ \mathbf{n} \in \mathbf{Z}^3\}$. The first expression is useful when t is large, and the second when t is small. Defining the truncated kernel

$$K_{lm}^{\mathbf{d},\lambda}(t, \mathbf{x}) = K_{lm}^{\mathbf{d}}(t, \mathbf{x}) - \sum_{\substack{\mathbf{r} \in P_d \\ |\mathbf{r}| < \lambda}} \mathcal{Y}_{lm}(\mathbf{r}) \exp(i\mathbf{r} \cdot \mathbf{x} - t\mathbf{r}^2) \tag{111}$$

it can be shown that the zeta function has a rapidly convergent integral expression

$$Z_{lm}^{\mathbf{d}}(1; q^2) = \sum_{\substack{\mathbf{r} \in P_d \\ |\mathbf{r}| < \lambda}} \frac{\mathcal{Y}_{lm}(\mathbf{r})}{\mathbf{r}^2 - q^2} + (2\pi)^3 \int_0^\infty dt \left(e^{tq^2} K_{lm}^{\mathbf{d},\lambda}(t, \mathbf{0}) - \frac{\gamma \delta_{l,0} \delta_{m,0}}{(4\pi)^2 t^{3/2}} \right). \tag{112}$$

In the integral above one uses the kernel expression (110) when $t < 1$, and (109) otherwise. The cutoff λ is chosen so that $\lambda^2 > \mathrm{Re}\, q^2$.

6 Conclusions

In this paper, we have developed a method that enables one to measure the elastic scattering phase shift with lattice Monte Carlo simulations when the total momentum of the scattering particles is non-zero. The method is an extension of the zero total momentum formalism, originally developed by Lüscher [12, 13], and it is based on the energy spectrum of the two-particle states in finite volumes.

We have applied the method to a 4-dimensional test model consisting of two Ising spin fields. By suitably choosing the parameters, the fields correspond to particles of two different masses, and by introducing a coupling between the fields the heavy particle appears as a resonance in the S-wave scattering channel of two light particles. We have shown excellent consistency between the rest frame and non-rest frame results and also the perturbation theory, and we have been able to extract the properties of the resonance to a good accuracy.

In our Monte Carlo simulations we have used a large number of lattice sizes and correspondingly a wide range of lattice momenta. This has enabled us to obtain a good

description of the phase shift function for the whole momentum range of interest separately for both the rest frame and the non-rest frame scattering sectors. However, often one has access only to a limited range of lattice sizes. Then the two momentum sectors complement each other: for a given lattice size, the center of mass frame energy and the relative momentum of the scattering particles is different in the total momentum $\mathbf{P} = 0$ and $\mathbf{P} = 2\pi/L$ sectors. Moreover, due to the kinematics of the scattering particles, the resonance usually appears at a smaller lattice size in the non-zero momentum sector than in the zero momentum sector. This can be a very significant factor when the lattice model is computationally so demanding that simulations in very large volumes are impractical.

As a final note, we consider the success of our work in this paper to be quite encouraging: we have obtained high-precision data for scattering phases in a 4-dimensional quantum field theory with only workstation-class computer simulations. It would be both interesting and challenging to apply these techniques to QCD.

References

[1] For recent reviews see D. Weingarten, Nucl. Phys. B (Proc. Suppl.) 34 (1994) 29; C. Michael, in Proceedings of Lattice '94, Nucl. Phys. B (Proc. Suppl.), to be published

[2] F. Butler, H. Chen, A. Vaccarino, J. Sexton, D. Weingarten, Nucl. Phys. B (Proc. Suppl.) 30 (1993) 377; Phys. Rev. Lett. 70 (1993) 2849

[3] S. Gottlieb, in Proceedings of Lattice '94, Nucl. Phys. B (Proc. Suppl.), to be published

[4] There is one case with a low quark mass and hard to fit rho propagator in which the effect of rho decay was suggested as a possible explanation. R. Altmeyer, K. D. Born, W. S. Ibes, E. Laermann, T. F. Walsh and P. M. Zerwas, UMN-TH-838/90

[5] S. Gottlieb, P. B. Mackenzie, H. B. Thacker and D. Weingarten, Phys. Lett. 134B (1984) 346; Nucl. Phys. B263 (1986) 704

[6] M. Guagnelli, E. Marinari and G. Parisi, Phys. Lett. B240 (1990) 188

[7] S. R. Sharpe, R. Gupta and G. W. Kilcup, Nucl. Phys. B393 (1992) 309

[8] R. Gupta, A. Patel and S. R. Sharpe, Phys. Rev. D48 (1993) 388

[9] Y. Kuramashi, M. Fukugita, H. Mino, M. Okawa, A. Ukawa, Phys. Rev. Lett. 71 (1993) 2383

[10] M. Fukugita, Y. Kuramashi, H. Mino, M. Okawa, A. Ukawa, Phys. Rev. Lett. 73 (1994) 2176; preprint KEK-CP-24 (1994)

[11] C. Bernard, T. Blum, T. A. DeGrand, C. DeTar, S. Gottlieb, A. Krasnitz, R. L. Sugar and D. Toussaint, Phys. Rev. D48 (1993) 4419

[12] M. Lüscher, Commun. Math. Phys. 104 (1986) 177; *ibid* 105 (1986) 153

[13] M. Lüscher, Nucl. Phys. B354 (1991) 531

[14] M. Lüscher, Nucl. Phys. B364 (1991) 237

[15] C. Michael, Nucl. Phys. B327 (1989) 515

[16] U.-J. Wiese, in Lattice '88, proc. 1988 symposium on lattice field theory, Batavia, Illinois (1988), ed. A. S. Kronfeld and P. B. Mackenzie, Nucl. Phys. B (Proc. Suppl.) 9 (1989) 609

[17] T. DeGrand, Phys. Rev. D43 (1991) 2296

[18] M. Lüscher and U. Wolff, Nucl. Phys. B339 (1990) 222

[19] C. R. Gattringer and C. B. Lang, Nucl. Phys. B391 (1993) 463

[20] H. R. Fiebig and R. M. Woloshyn, Nucl. Phys. B (Proc. Suppl.) 30 (1993) 883

[21] H. R. Fiebig, R. M. Woloshyn and A. Dominiguez, Nucl. Phys. B 418 (1994) 649

[22] M. Göckeler, H. A. Kastrup, J. Westphalen, F. Zimmermann, Nucl. Phys. B425 (1994) 413

[23] M. Göckeler, H. A. Kastrup, J. Viola and J. Westphalen, talk given in Lattice '94 conference, preprint HLRZ Jülich 94–47

[24] M. Lüscher and P. Weisz, Nucl. Phys. B290 [FS20] (1987) 25; B295 [FS21] (1988) 65

[25] I. Montvay and P. Weisz, Nucl. Phys. B290 [FS20] (1987) 327

[26] I. Montvay, G. Münster, P. Weisz, Nucl. Phys. B305 [FS23] (1988) 143

[27] D. S. Gaunt, M. F. Sykes and S. McKenzie, J. Phys. A12 (1979) 871

[28] R. H. Swendsen and J.-S. Wang, Phys. Rev. Lett. 58 (1987) 86

[29] J. Hoshen and R. Kopelman, Phys. Rev. B14 (1976) 3438

[30] See, for example, L. D. Landau and E. M. Lifshitz, *Quantum Mechanics*, 3rd edition, Pergamon Press, 1959

[31] M. Weissbluth, *Atoms and Molecules*, Academic Press, New York (1978)

[32] M. Rotenberg, R. Bivins, N. Metropolis, and K. Wooten, Jr., *The 3j and 6j symbols*, MIT Press, Cambridge, Massachusetts (1959)